ADVANCING EARTH AND SPACE SCIENCE

Geochemistry, Geophysics, Geosystems

RESEARCH ARTICLE
10.1029/2020GC009199

Key Points:

- The tectono-magmatic evolution recorded at the Mado Megamullion recalls that of mid-ocean ridge oceanic core complexes
- Lower oceanic crust in back-arc basins shows a distinctive crystal line of descent triggered by the water-rich character of the melt
- Phase assemblages in oceanic gabbros can be used as a diagnostic for the tectonic setting of formation of lower crustal rocks in ophiolites

Supporting Information:

- Table S1
- Table S2
- Table S3
- Table S4
- Table S5
- Table S6

Correspondence to:
V. Basch,
valentin.basch@gmail.com

Citation:
Basch, V., Sanfilippo, A., Sani, C., Ohara, Y., Snow, J., Ishizuka, O., et al. (2020). Crustal accretion in a slow spreading back-arc basin: Insights from the Mado Megamullion oceanic core complex in the Shikoku Basin. *Geochemistry, Geophysics, Geosystems*, *21*, e2020GC009199. https://doi.org/10.1029/2020GC009199

Received 27 MAY 2020
Accepted 6 SEP 2020
Accepted article online 11 SEP 2020

Crustal Accretion in a Slow Spreading Back-Arc Basin: Insights From the Mado Megamullion Oceanic Core Complex in the Shikoku Basin

V. Basch[1], A. Sanfilippo[1], C. Sani[1], Y. Ohara[2,3,4], J. Snow[5], O. Ishizuka[3,6], Y. Harigane[6], K. Michibayashi[4], A. Sen[7], N. Akizawa[8], K. Okino[8], M. Fujii[9], and H. Yamashita[10]

[1]Dipartimento di Scienze della Terra e dell'Ambiente, University of Pavia, Pavia, Italy, [2]Department of Japan, Hydrographic and Oceanographic, Tokyo, Japan, [3]Japan Agency for Marine-Earth Science and Technology, Yokosuka, Japan, [4]Department of Earth and Planetary Sciences, Nagoya University, Nagoya, Japan, [5]Department of Geology and Geophysics, Louisiana State University, Baton Rouge, LA, USA, [6]Institute of Geology and Geoinformation, Geological Survey of Japan, National Institute of Advanced Industrial Science and Technology, Tsukuba, Japan, [7]Earth and Atmospheric Sciences Department, University of Houston, Houston, TX, USA, [8]Atmosphere and Ocean Research Institute, University of Tokyo, Tokyo, Japan, [9]National Institute of Polar Research, Tachikawa, Japan, [10]Kanagawa Prefectural Museum of Natural History, Odawara, Japan

Abstract Oceanic core complexes (OCCs) represent tectonic windows into the oceanic lower crust and mantle; they are key structures in understanding the tectono-magmatic processes shaping the oceanic lithosphere. We present a petrological and geochemical study of gabbros collected at the Mado Megamullion, a recently discovered OCC located in the extinct Shikoku back-arc basin. Bathymetry of the Mado Megamullion reveals spreading-parallel corrugations extending 25 km from the breakaway to the termination. Samples from several locations include peridotites, gabbros, dolerite, and rare pillow basalts. Gabbros range from granular to varitextured olivine gabbros and oxide gabbros. The emplacement of these gabbroic rocks within the oceanic lithosphere was followed by a multiphase tectono-metamorphic evolution including (i) dynamic recrystallization within shear zones, developed under granulite- to upper-amphibolite-facies conditions, and (ii) intrusion of highly evolved melts forming felsic segregations. This tectono-metamorphic evolution recalls that of the lower crust from other OCCs worldwide, demonstrating that this OCC exposes deep-seated intrusions progressively exhumed by detachment faulting. Nonetheless, the Mado Megamullion lower crustal gabbros show an unusual crystal line of descent, different from what is reported from mid-ocean ridge lower crustal rocks. We infer that the water-bearing character of the primary melts in this back-arc basin triggered the early precipitation of clinopyroxene, soon followed by amphibole and Fe-Ti oxides. Such modifications in phase saturation are likely to be directly related to the back-arc setting of the Mado Megamullion. If so, the phase assemblages of oceanic gabbros may be a diagnostic for the tectonic setting of lower crustal rocks in ophiolites.

1. Introduction

Formation of oceanic crust represents the main contribution of mass flow from the Earth's interior to the surface, as it accounts for 88% of global Earth surface produced over time (Bird, 2003). A significant fraction of seafloor spreading takes place in back-arc environments, where water has long been known to play a major role in generating back-arc basin basalts, a striking contrast to the relatively dry magmas erupting at mid-ocean ridges (e.g., Sdrolias & Müller, 2006; Taylor & Martinez, 2003). Moreover, much of our understanding of the deeper oceanic crust derives from the study of ophiolites. Most of these while mostly attributed to suprasubduction zone environments (e.g., Pearce, 2003) do not generally have a clearly defined original tectonic setting. Thus, the igneous processes and mantle dynamics specific to back-arc seafloor spreading are yet to be fully explored.

Oceanic core complexes (OCCs) are topographic highs that form by extension and uplift during periods of reduced magma supply, usually at the intersection between a transform fault and a spreading ridge (Ildefonse, Blackman, et al., 2007; MacLeod et al., 2009; Olive et al., 2010). They represent exhumed footwall of long-lived oceanic detachment faults and therefore give direct access to the lowermost oceanic crust and mantle peridotites. OCCs are commonly used as tectonic windows to investigate the deep igneous processes shaping the oceanic lithosphere and to overcome the difficulty of deep oceanic drilling (Dick et al., 2006; Ildefonse, Christie, & Mission Moho Workshop Steering Committee, 2007). They have been first identified along the Mid-Atlantic Ridge (Blackman et al., 1998; Cann et al., 1997; Karson, 1990; Tucholke et al., 1998; Tucholke & Lin, 1994) and are characterized by a domal surface, spreading-parallel surface corrugations and high mantle Bouguer anomaly related to the shallow occurrence of lower crustal and mantle material (Blackman et al., 1998; MacLeod et al., 2009; Tucholke et al., 1998). They have been documented mostly in slow to ultraslow spreading environments such as the Mid-Atlantic Ridge (e.g., Blackman et al., 2011; Dick et al., 2008; Escartìn et al., 2008; Kelemen et al., 2004; MacLeod et al., 2009; Parnell-Turner et al., 2018; Smith et al., 2008, 2014) and the Southwest Indian Ridge (e.g., Dick et al., 2002; Dick, Kvassnes, et al., 2019; Dick, MacLeod, et al., 2019; Sauter et al., 2013). In back-arc spreading environments, the only presently documented OCC is the Godzilla Megamullion in the Parece Vela Basin (e.g., Ohara, 2016), the largest OCC discovered to date, approximately 10 times larger than those commonly found along the Mid-Atlantic Ridge (Ohara et al., 2003). Although the study of the Godzilla Megamullion has contributed to understanding the igneous processes and mantle dynamics leading to back-arc spreading, it calls for the study of new tectonic windows in back-arc settings, in order to constrain the evolution of the oceanic lithosphere during the formation of back-arc basins.

We here introduce the Mado Megamullion, a back-arc OCC recently identified in the Shikoku Basin (Ohara et al., 2018). The Mado Megamullion is only 1,300 km from Tokyo, Japan (~2 days transit), therefore making it an easily accessible tectonic window in the world's oceans (*Mado* stands for *Window* in Japanese). This paper briefly documents the overall structure of the Mado Megamullion OCC and mostly focuses on the petrography and chemical composition of the gabbroic samples collected by submersible and dredging. Comparison of the structure and composition of the gabbroic crust is made with other OCCs worldwide, with special focus on the Atlantis Bank. Indeed, the latter involved similar spreading rates during OCC formation and presents widespread occurrence of oxide gabbros, felsic veins, and high-temperature mylonitic shear zones.

2. Geological Setting

The Mado Megamullion is located in the southernmost Shikoku Basin (Figure 1a) at ~23°50′N, a NNW-SSE trending extinct back-arc basin, which was actively spreading from 27 to 15 Ma (Ishizuka et al., 2009; Kobayashi et al., 1995; Okino et al., 1994, 1999; Sdrolias et al., 2004; Taira et al., 2016). It separates the Kyushu-Palau Ridge from the West Mariana Ridge and is in continuity to the south with the Parece Vela Basin (Figure 1a), with which it shares a common evolution (Okino et al., 1999; Sdrolias et al., 2004; Taira et al., 2016). Back-arc spreading was associated with the subduction of the western margin of the Pacific Plate; the Shikoku Basin formed in two stages, from ENE-WSW spreading (27–19 Ma, 35 mm/year) to NE-SW spreading (19–15 Ma, 7 mm/year) (Okino et al., 1994, 1998, 1999; Sdrolias et al., 2004). The central Shikoku and Parece Vela Basins have a zigzag geometry of mostly orthogonal spreading axes, consisting of a series of short length (~20 to ~55 km) first-order segments aligned en echelon with closely spaced fracture zones (Figure 1a; Ohara et al., 2001). Okino et al. (1999) described a notable difference in the axial morphology between the Shikoku and Parece Vela Basins: a series of seamounts formed by postspreading volcanism, known as the Kinan Seamount Chain, are found in the axial Shikoku Basin, while a series of deep rifts, known as the Parece Vela Rift, occupy the axial Parece Vela Basin. The southernmost Shikoku Basin axis also consists of deep rifts, apparently sharing the morphological characteristics of the Parece Vela Basin axis (Figure 1a; Ohara et al., 2001; Okino et al., 1999).

Extensive multibeam bathymetric mapping by Japan's continental shelf survey revealed the potential presence of OCCs in the Shikoku and Parece Vela Basins (Ohara et al., 2015). Accordingly, the Godzilla Megamullion was documented in 2001 in the Parece Vela Basin (~16°N; Harigane et al., 2008, 2010, 2011, 2019; Loocke et al., 2013; Michibayashi et al., 2014, 2016; Ohara, 2016; Ohara et al., 2001, 2003, 2011; Ohara & Snow, 2009; Sanfilippo et al., 2013, 2016; Spencer & Ohara, 2014; Tani et al., 2011). It is the largest OCC structure in the world (55 km along-segment, 125 km ridge-perpendicular) and presents topographic corrugations indicative of long-lived detachment faulting and heterogeneous lithologies varying from exposed mantle peridotites to massive gabbroic bodies, diabase, and basalts (e.g., Ohara, 2016). The Godzilla Megamullion is interpreted to have formed by long-lived detachment faulting in a slow

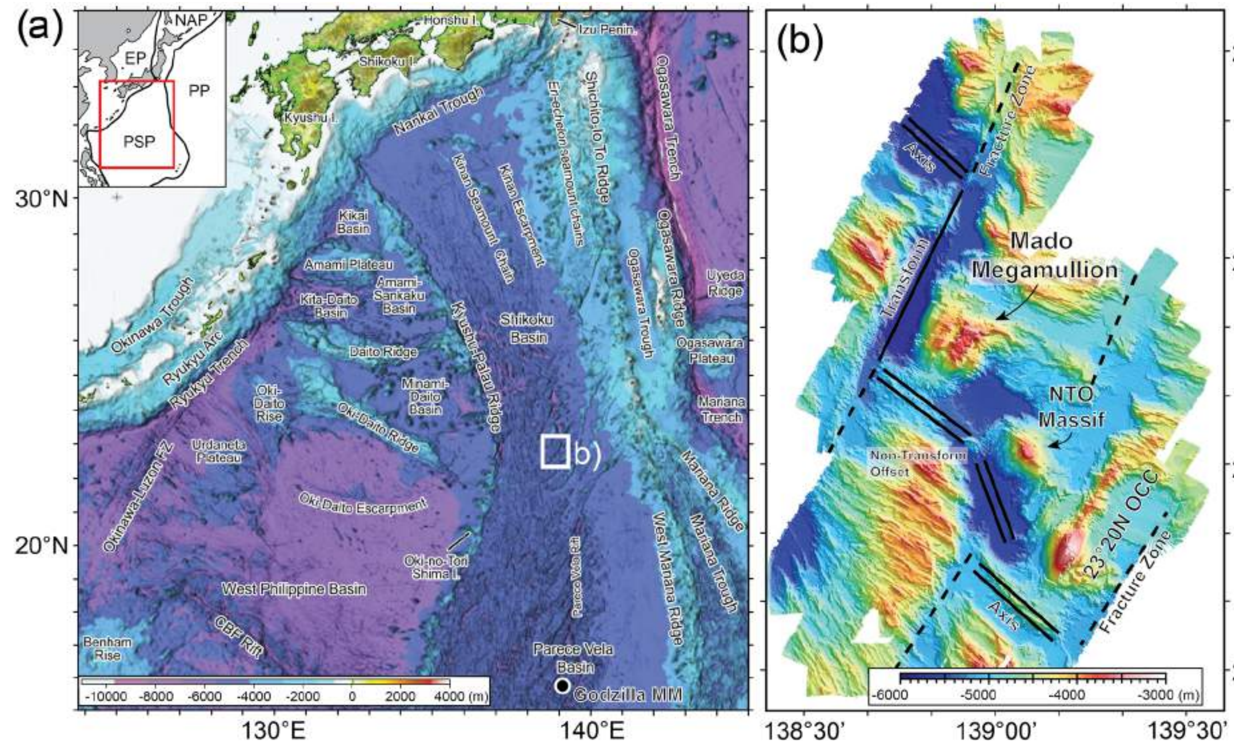

Figure 1. (a) Bathymetric map of the Shikoku Basin, after Taira et al. (2016). The top left inset shows the plate tectonic settings of the studied area; EP = Eurasian plate; PP = Pacific plate; PSP = Philippine Sea plate; NAP = North American plate. The white square indicates the location of the Mado Megamullion and the black dot locates the Godzilla Megamullion (see Ohara, 2016). (b) Interpretative bathymetric map of the Mado Megamullion. Double lines indicate inactive spreading segments, single line indicates transform faults, and dashed lines indicate fracture zones.

spreading environment (Tani et al., 2011), similar to OCCs exposed at modern slow and ultraslow spreading ridges (Escartìn et al., 2008; Ildefonse, Blackman, et al., 2007; MacLeod et al., 2009), and so far represents the only well-studied OCC in back-arc oceanic lithosphere.

Multibeam bathymetry, gravimetric surveys, and sampling of the area included between 23°N to 24°30′N and 138°30′E to 139°30′E, in the southernmost Shikoku Basin, revealed the presence of three distinct topographic highs exposing mantle peridotites (Figure 1b), namely, (i) the *Mado Megamullion*, located at an inside corner of a ridge-transform intersection (23°50′N, 138°50′E) and having spreading-parallel corrugations extending for 24 km from the breakaway to the termination, with a total extent of the corrugated surface of ~500 km^2, yielding serpentinized peridotite and gabbro, and positive mantle Bouguer anomalies (Ohara et al., 2018; Okino et al., 2019); (ii) the *Non-Transform Offset* (NTO) *Massif* (23°30′N, 139°05′E), a bathymetric high yielding serpentinized peridotite and characterized by positive mantle Bouguer anomalies (Ohara et al., 2018; Okino et al., 2019) but lacking prominent corrugations; (iii) the 23°20′N *OCC* (139°10′E), an elongated spreading-parallel topographic high yielding serpentinized peridotite, located at the center of the ridge segment. Although not associated with positive mantle Bouguer anomalies (Ohara et al., 2018; Okino et al., 2019), this feature presents spreading-parallel corrugations. The present study focuses on the gabbros collected at the Mado Megamullion.

3. Lower Crust at the Mado Megamullion

The Mado Megamullion was first sampled by a reconnaissance cruise in 2007 (R/V Hakuho-maru KH07-02), recovering a small amount of serpentinized peridotite. In 2018, two cruises mapped and sampled it by dredging (R/V Hakuho-maru KH18-2) and by DSV Shinkai 6500 (R/V Yokosuka YK18-07) (Ohara et al., 2018). In 2019, another cruise was conducted (R/V Yokosuka YK19-04S), performing detailed geophysical mapping as well as sampling and near-seafloor geophysical mapping with DSV Shinkai 6500 of the OCC (Figures 2a and 2b). Sample collection includes sediments, serpentinized peridotites, variably evolved and deformed gabbroic rocks, and minor pillow basalts and decimeter-size doleritic intrusions (Figure 2c)

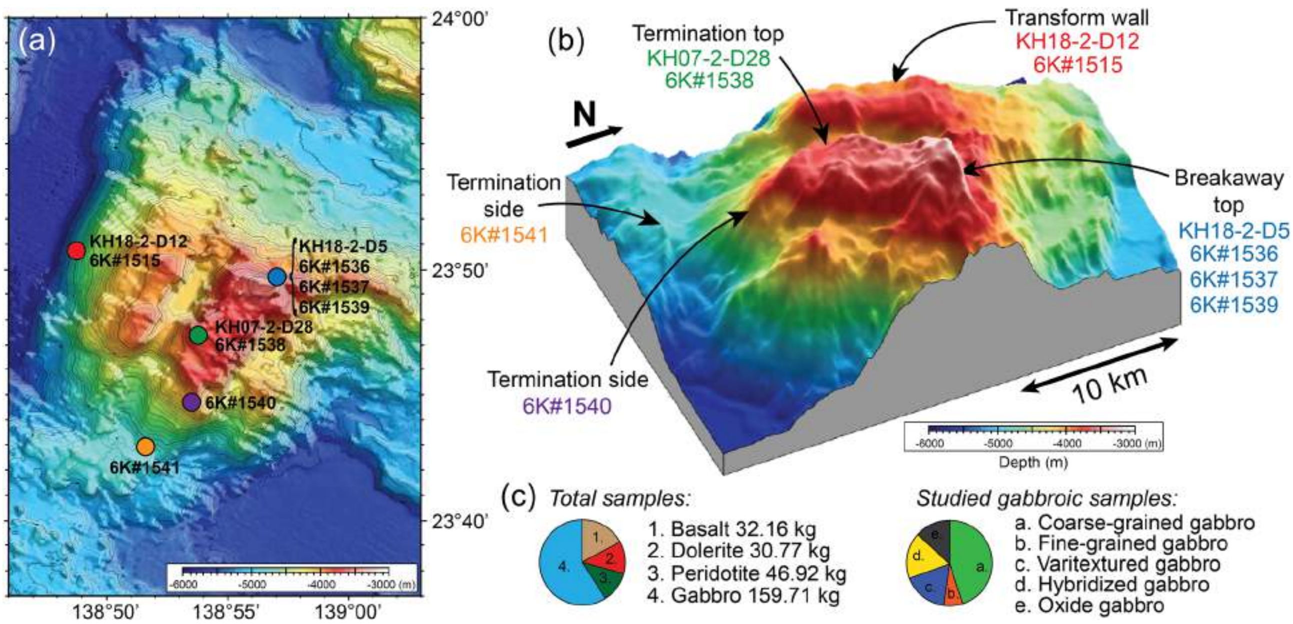

Figure 2. (a) Detailed bathymetric map of the Mado Megamullion, showing the location of dredge sites and dives that recovered the studied samples; (b) 3-D morphological view of the Mado Megamullion; (c) total key samples and gabbroic rocks recovered.

(Ohara et al., 2019). The sedimentary cover did not allow for field mapping of intrusions and veins during DSV Shinkai 6500 dives. A detailed discussion of the morphological features and the results of geophysical surveys will be presented in a separate study; we here focus on the gabbroic rocks.

4. Main Petrographic Features

Collected gabbros range from relatively primitive coarse- to fine-grained olivine gabbros, locally showing "varitextured" characteristics and highly evolved oxide gabbros (Figures 3a and 3b). The olivine-gabbros are widely crosscut by felsic veins (Figure 3). The primitive gabbros were sampled both at the breakaway and termination areas, whereas the oxide gabbros were exclusively recovered along the transform wall (Figures 2a and 2b; see Table 1 for details).

4.1. Olivine Gabbros

The olivine gabbros show variations in modal composition, texture, and deformation intensity, ranging from coarse-grained gabbro to fine-grained gabbro, varitextured gabbro, and sheared gabbro. Primary contacts between these gabbroic lithotypes were not sampled in place, and they will be hereafter described separately. Nearly all collected samples are crosscut by a network of subparallel millimeter-thick veins filled by ~100 μm-sized dark-green amphibole, which are associated with alteration halos in the host gabbros; the latter are characterized by amphibole coronas around magmatic clinopyroxene and very fine-grained albitic plagioclase replacing large magmatic plagioclase.

1. *Coarse-grained olivine gabbros* are characterized by hypidiomorphic textures of millimeter-size crystals of subhedral olivine (2–10 vol%), plagioclase (50–65 vol%), and interstitial to poikilitic clinopyroxene (30–40 vol%) (Figure 4a). Brown amphibole is commonly present as subhedral grains to small interstitial phase at the contact between plagioclase and clinopyroxene, clearly evidencing a magmatic origin (~2–3 vol%). Primary phases are widely replaced by late-stage mineral associations; olivine is extensively altered into a mesh texture of serpentine and magnetite, and fresh cores are rarely preserved; plagioclase is often recrystallized into fine-grained aggregates exhibiting triple grain junctions, and clinopyroxene is intensely substituted by dark- to light-green amphibole (Figure 4a).
2. *Fine-grained olivine gabbros* are characterized by granular, submillimetric crystals of olivine (<5 vol%), subprismatic plagioclase (45–50 vol%), granular clinopyroxene (40–45 vol%), and subhedral brown amphibole (~5%; Figure 4b). Plagioclase is well preserved whereas clinopyroxene is intensely

10.1029/2020GC009199

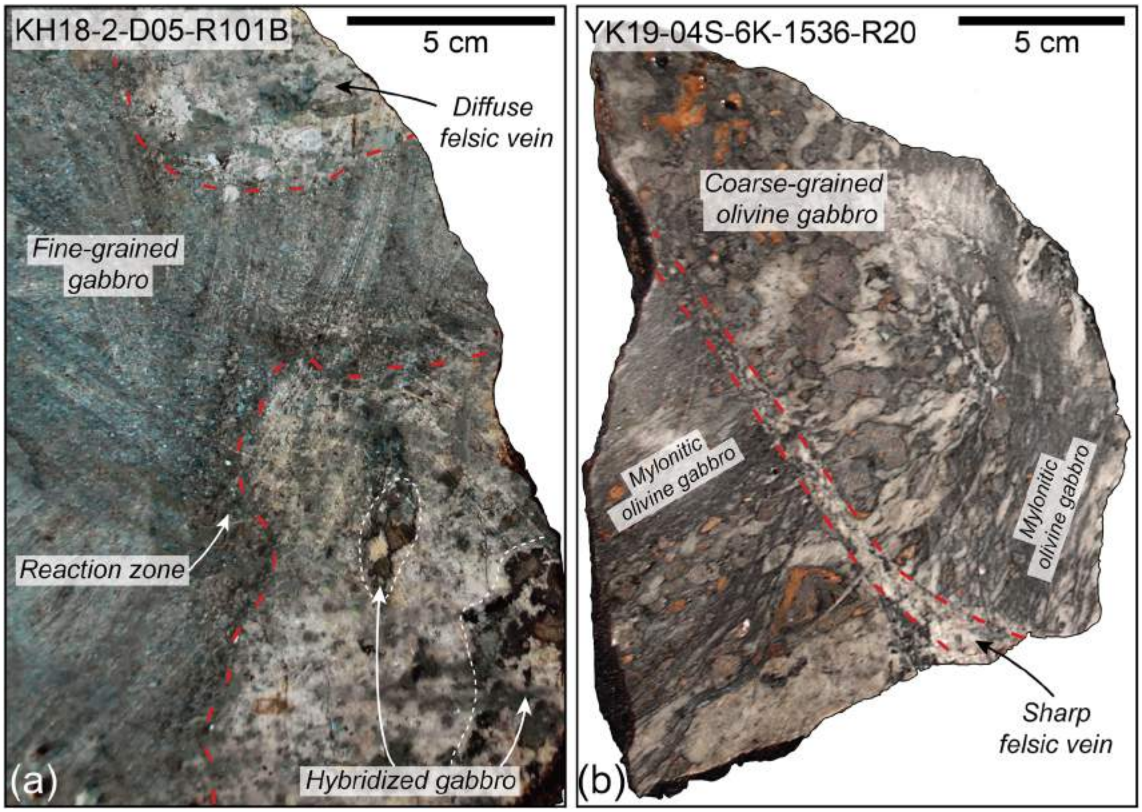

Figure 3. Hand sample photographs of (a) fine-grained gabbro crosscut by diffuse felsic vein, in places including centimeter-size lenses of hybridized gabbros. The latter correspond to the reacted host rock crosscut and enclosed in a network of felsic material. The contact between the diffuse felsic vein and the host gabbro is characterized by an amphibole + oxide reaction zone; (b) coarse-grained to mylonitic olivine gabbro crosscut by a centimeter-thick sharp felsic vein. It is noteworthy that the felsic vein is associated with displacement of the host olivine gabbro.

substituted by dark-green amphibole. Figure 4b shows subparallel millimeter-thick dark-green amphibole-rich veins crosscutting the fine-grained gabbro.

3. *Varitextured olivine gabbros* show granular domains similar to those of the coarse-grained gabbros but in places millimeter-size rounded patches of ~40–45 vol% fine-grained plagioclase, ~40–45 vol% clinopyroxene associated with ~10–15 vol% interstitial brown amphibole (Figures 4c and 4d) are present. Similar textures have been described at the gabbro-dike transition from the East Pacific Rise (IODP Hole 1256D; Koepke et al., 2011) and Oman Ophiolite (France et al., 2009) and were interpreted as frozen melts crystallized in situ at the borders of axial melt lenses.
4. *Sheared olivine gabbros*: Most olivine gabbros show textural evidence for crystal-plastic deformation, such as the occurrence of porphyroclasts with undulose extinction and kink bands surrounded by well-equilibrated fine-grained neoblasts. In discrete zones, the deformation intensity grades from porphyroclastic to mylonitic (Figure 3b). Gabbroic mylonites are found as centimeter- to decimeter-thick bands within olivine gabbros (Figure 3b) and were distinguished on the basis of the neoblastic mineralogical associations into (i) granulite-facies mylonite and (ii) amphibolite-facies mylonite (see section 6.2 for geothermometric estimates). They are characterized by a well-defined foliation and by the association of fine-grained recrystallized plagioclase and mafic aggregates made of (i) brown amphibole + clinopyroxene in granulite-facies mylonites (Figure 4f) and (ii) brown to dark-green amphibole + Fe-Ti oxides in amphibolite-facies mylonite (Figure 4g). The mafic aggregates in both mylonite types often preserve relict clinopyroxene porphyroclasts that, in the case of the amphibolite-facies mylonites, also show widespread substitution by dark- to light-green amphibole (Figures 4e and 4g).

4.2. Oxide Gabbros

Oxide gabbros (12–20 vol% Fe-Ti oxides) have been exclusively sampled at the transform wall (Figures 2a and 2b). All such samples are deformed with a well-defined porphyroclastic foliation formed of sigmoidal

10.1029/2020GC009199

Table 1
Studied Samples and Sampling Location on the Mado Megamullion

					Modal compositions (vol%)					
Sample	Lithotype	Depth	Latitude	Longitude	Ol	Plg	Cpx	Ox	Amph	Petrographic observation
KH18-2-D05R101B3	Fine-grained gabbro	4,522	23°51.7310′N	138°57.8930′E	4	46	44	1	5	Amph-rich vein
YK19-04S-6K1536R14	Coarse-grained olivine gabbro	3,608	23°49.7226′N	138°56.6931′E	2	62	34	0	2	—
YK19-04S-6K1536R16	Coarse-grained olivine gabbro	3,608	23°49.7226′N	138°56.6931′E	6	51	39	1	3	Amph-rich vein
YK19-04S-6K1536R18	Coarse-grained olivine gabbro	3,540	23°49.6782′N	138°56.6738′E	10	50	35	2	3	—
YK19-04S-6K1536R20	Mylonitic olivine gabbro	3,498	23°49.6532′N	138°56.6656′E	7	48	30	2	13	Cpx-myl.; Sharp felsic vein; Amph-rich vein
KH18-2-D05R101A1	Varitextured gabbro	4,522	23°51.7310′N	138°57.8930′E	1	58	36	0	5	Sharp felsic vein; Amph-rich vein
KH18-2-D05R101A4	Varitextured gabbro	4,522	23°51.7310′N	138°57.8930′E	2	47	43	1	7	Mm-size patches
YK19-04S-6K1536R10	Hybridized gabbro	3,760	23°49.8219′N	138°56.7271′E	0	46	42	4	8	Diffuse felsic mat.
KH18-2-D05R101A2	Hybridized gabbro	4,522	23°51.7310′N	138°57.8930′E	0	68	21	3	8	Diffuse felsic mat.
KH18-2-D05R101B1	Hybridized gabbro	4,522	23°51.7310′N	138°57.8930′E	0	71	13	7	9	Diffuse felsic mat.; Amph. myl.
KH18-2-D05R101B2	Hybridized gabbro	4,522	23°51.7310′N	138°57.8930′E	1	58	28	6	7	Diffuse contact felsic mat.-fine-gr. gabbro
YK19-04S-6K1538-501A	Hybridized gabbro	3,696	23°47.4335′N	138°53.8434′E	1	54	40	1	4	Diffuse felsic mat.
KH18-2-D12-R101	Oxide gabbro	5,403	23°49.3060′N	138°47.6350′E	0	40	34	16	10	—
KH18-2-D12-R107	Oxide gabbro	5,403	23°49.3060′N	138°47.6350′E	0	47	28	20	5	Amph. myl.; Amph-rich vein
KH18-2-D12-R111	Oxide gabbro	5,403	23°49.3060′N	138°47.6350′E	0	42	32	17	9	Amph. myl.
YK18-07-6K1515R14	Oxide gabbro	5,073	23°50.4372′N	138°48.3942′E	0	44	36	12	8	—
YK18-07-6K1515R04	Oxide gabbro	5,599	23°50.6100′N	138°47.9940′E	0	51	27	15	7	Amph. myl.; Amph-rich vein
YK18-07-6K1515R12	Dolerite intrusion	5,162	23°50.4648′N	138°48.3606′E	0	56	39	4	1	—

Note. Cpx-myl. = clinopyroxene-bearing mylonite; Amph. myl. = amphibole-rich mylonite; Fine-gr. gabbro = fine-grained gabbro.

centimeter-size altered clinopyroxenes, Fe-Ti oxides (ilmenite, magnetite up to 30–40 vol%), and plagioclase (60–70 vol%). The porphyroclasts are partly recrystallized into plagioclase + amphibole + oxide neoblastic aggregates (Figure 5a). Amphibolite-facies mylonitic recrystallization is also observed in these oxide gabbros, where fine-grained aggregates of brown to dark-green amphibole and Fe-Ti oxides locally crystallize around the porphyroclastic clinopyroxene. Notably, oxide gabbros are neither crosscut nor physically associated with felsic veins.

4.3. Felsic Veins

Olivine gabbros are widely crosscut by felsic veins showing sharp to diffuse contacts with the host rock (Figures 3a and 3b). The felsic material locally intrudes and disrupts the existing gabbroic framework to form centimeter-size lenses of gabbros completely surrounded by felsic material, hereafter called "hybridized gabbros" (Figure 3a). The felsic veins are centimeter to decimeter in size and locally crosscut the high-temperature crystal-plastic fabric at high angles (Figures 3b and 4e).

1. *Sharp felsic veins* are characterized by straight contacts with the host gabbro and show limited chemical interaction between the melts forming the vein and the host rock (Figure 5b). The veins are formed by euhedral, optically zoned albitic plagioclase up to millimeters in size (80 vol%) and interstitial to subhedral brown amphibole (up to 20 vol%), widely replaced by late-stage green amphibole. Sample YK19-04S-6K-1536-R20 contains an undeformed sharp felsic vein that forms the contact between a nearly undeformed gabbro and a granulite-facies mylonite (Figures 3b and 5b). This suggests that the felsic vein was emplaced in a preexisting fracture involving displacement within the host rock or that the displacement occurred during intrusion.
2. *Diffuse felsic veins* are characterized by diffuse, gradational contacts with the host gabbro marked by a millimeter-thick reaction zone (Figure 5c). The reaction zone is made of poikilitic brown amphibole enclosing Fe-Ti oxides (ilmenite and magnetite) and apatite. Away from the contact, the vein is

10.1029/2020GC009199

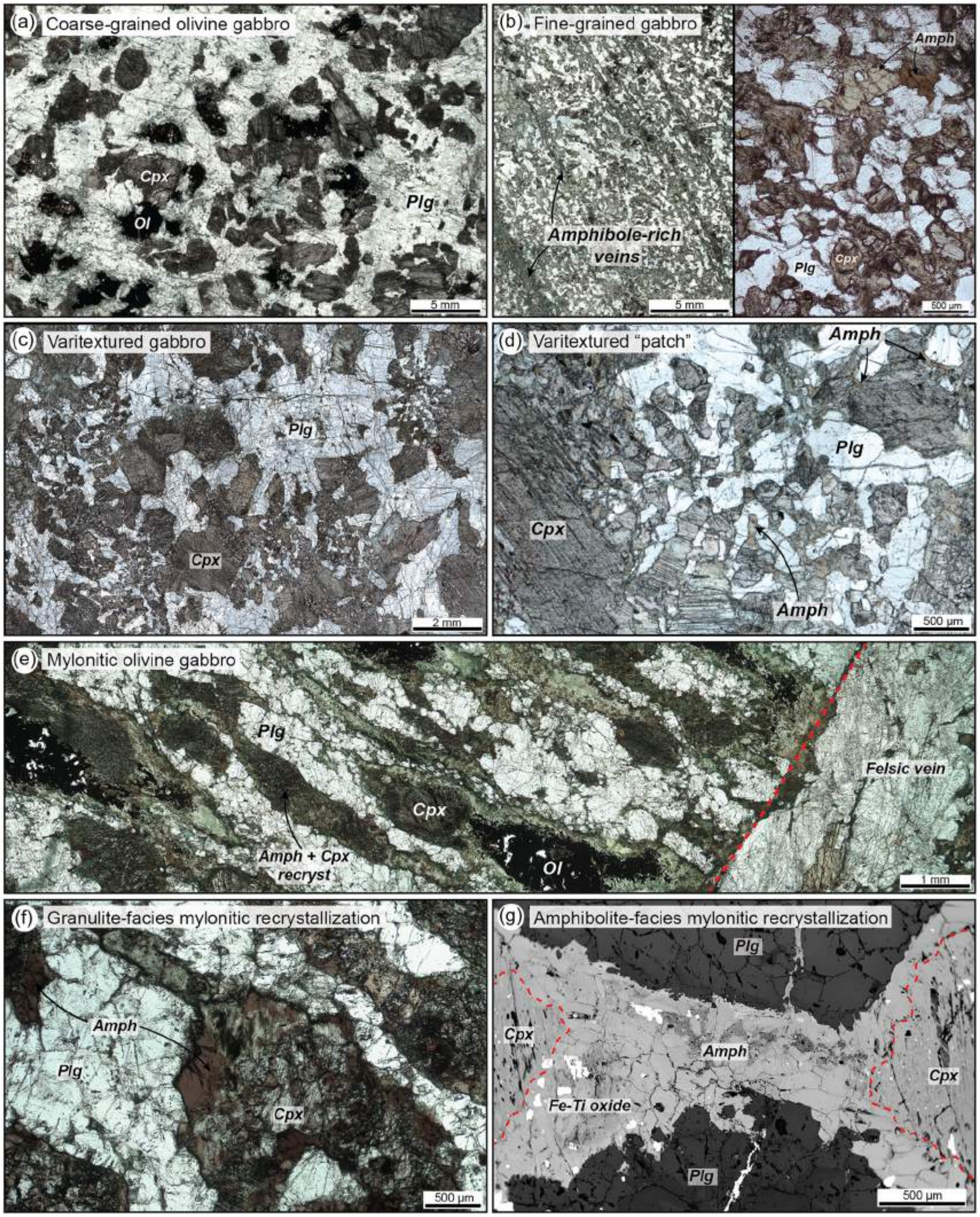

Figure 4. Photomicrographs of representative microstructures of the studied gabbroic lithotypes. (a) Coarse-grained olivine gabbro; (b) fine-grained gabbro and detail of the amphibole-bearing mineralogical assemblage; (c) varitextured gabbro; (d) close-up of an amphibole-bearing varitextured patch; (e) mylonitic olivine gabbro crosscut by a sharp felsic vein; (f) granulite-facies mylonitic recrystallization within a deformed olivine gabbro; (g) back-scattered electron image of amphibolite-facies mylonitic recrystallization within a deformed hybridized gabbro.

formed of millimeter-size euhedral plagioclase (80 vol%), in places enclosed within poikilitic brown amphibole (up to 20 vol%) (Figure 5c).

3. *Hybridized gabbros* are centimeter-size lenses included within a framework of felsic material. They are formed of the same assemblages found as reaction products between the felsic melt and host gabbro. Where preserved, the original clinopyroxenes are partly corroded and rimmed by thick reaction

10.1029/2020GC009199

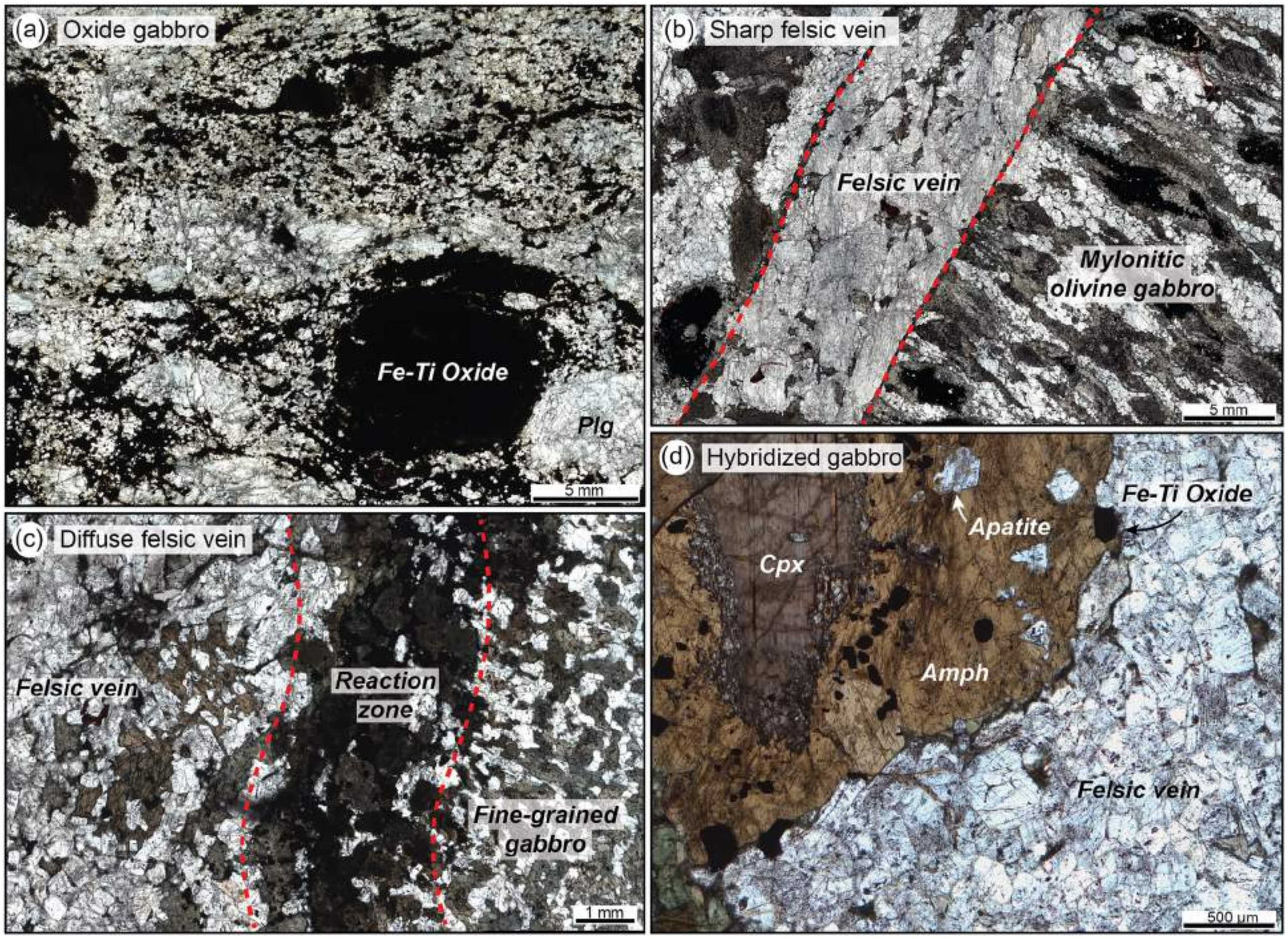

Figure 5. Representative microstructures of the lithotypes associated with felsic intrusions. (a) Deformed oxide gabbro; (b) felsic vein showing sharp contacts with host gabbros, intruded at the contact between a mylonitic olivine gabbro and an undeformed olivine gabbro; (c) diffuse felsic vein and [amphibole + oxide + apatite] reaction zone at the contact with the host fine-grained gabbro; (d) [amphibole + oxide + apatite] reaction rim around a relitic clinopyroxene, within a hybridized gabbro.

coronas formed of brown amphibole + Fe-Ti oxides + apatite (Figures 3a and 5d). Plagioclase develops a strong chemical zoning (see section 6.1) and commonly show recrystallized albitic grains. Large brown amphibole also occurs as poikilitic grains including subhedral albitic plagioclase. The hybridized gabbros locally preserve deformed portions, characterized by mylonitic recrystallization commonly developed under amphibolite-facies. These deformed portions, surrounded by undeformed felsic material, show fine-grained aggregates of brown amphibole and Fe-Ti oxides recrystallizing at the expense of porphyroclastic clinopyroxene.

4.4. Dolerite

The single dolerite sample is characterized by centimeter-size clinopyroxene and plagioclase phenocrysts enclosed in an ophitic fine-grained matrix of elongated euhedral plagioclase, granular clinopyroxene, Fe-Ti oxides, and rare orthopyroxene and apatite. The contact between the doleritic intrusion and the host rock was not sampled, but the rapid cooling leading to the crystallization of the fine-grained ophitic matrix suggests the emplacement of the intrusion in a cold, brittle host rock.

5. Analytical Methods

Mineral major element Electron Probe Micro-Analyses (EPMA) were performed on 18 samples, including 7 olivine gabbros bearing felsic veins (3 coarse-grained olivine gabbros, 1 fine-grained gabbros, 2 varitextured gabbros, and 1 mylonitic olivine gabbro), 5 hybridized gabbros, 5 oxide gabbros, and 1 doleritic intrusion

(Table 1). Major element (SiO_2, TiO_2, Al_2O_3, Cr_2O_3, FeO, MgO, MnO, CaO, NiO, Na_2O, K_2O, and ClO_2) compositions of olivine, clinopyroxene, plagioclase, and amphibole were analyzed by JEOL JXA 8200 Superprobe equipped with five wavelength-dispersive (WDS) spectrometers, an energy dispersive (EDS) spectrometer, and a cathodoluminescence detector (accelerating potential 15 kV, beam current 15 nA), operating at the Dipartimento di Scienze della Terra, University of Milano. The analyses of all elements were performed with a 30 s counting time.

Whole rock chemistry of Mado Megamullion basalts (Table S1 in the supporting information) was determined at the Geological Survey of Japan/AIST following the method described in Ishizuka et al. (2020). Major elements were analyzed on glass beads, prepared by fusing 1:10 mixtures of 0.5 g subsamples and lithium tetraborate. The glass beads were analyzed using a Panalytical Axios XRF spectrometer. External uncertainty and accuracy are generally <2% (2σ standard deviation), but Na shows as much as ~7% analytical uncertainty. The rare-earth elements (REE), V, Cr, Ni, Rb, Sr, Y, Zr, Nb, Cs, Ba, Hf, Ta, Pb, Th, and U concentrations were analyzed by ICP-MS on an Agilent 7900 instrument. About 100 mg of powder from each sample was dissolved in a HF-HNO_3 mixture (5:1) using screw-top Teflon beakers. Instrument calibration was performed using five to six calibration solutions made from international rock standard materials (including BIR-1, BCR-1, AGV-1, JB1a, and BEN). Reproducibility is generally better than ±4% (RSD) for the REE and better than ±6% (RSD) for other elements, except those with very low concentration and Ni (see BHVO2 analysis in Ishizuka et al., 2020). Loss on ignition (LOI) was determined for both samples and yield rather low values (3.20–3.42 wt%; Table S1).

6. Results

6.1. Mineral Major Element Compositions

Major element compositions of olivine, clinopyroxene, plagioclase, and amphibole from the Mado Megamullion gabbroic crust are reported in Tables S2–S5.

Olivine is extensively altered and was analyzed only in the coarse-grained olivine gabbro (Sample 6K-1536-R18). It shows evolved compositions with Fo = 75.5–76.0 mol% (Fo = Mg/[Mg + Fe^{2+}]) and NiO = 0.06–0.11 wt%.

Clinopyroxene (Figure 6) shows rather homogeneous compositions in the olivine gabbros (Mg# = 81.0–85.5 mol%; Al_2O_3 = 1.34–3.5 wt%; TiO_2 = 0.30–0.73 wt%; Cr_2O_3 = 0.02–0.45 wt%; Na_2O = 0.21–0.62 wt%), similar to clinopyroxene compositions in the Atlantis Bank olivine gabbros (Southwest Indian Ridge; Dick et al., 2002). Clinopyroxenes in oxide gabbros show a large compositional range, with more evolved compositions (Mg# = 59.9–73.7 mol%; Al_2O_3 = 0.9–2.4 wt%; TiO_2 = 0.16–0.69 wt%; Cr_2O_3 = 0.01–0.06 wt%; Na_2O = 0.26–0.88 wt%). They show low Al_2O_3 and TiO_2 at high Mg values, respect to clinopyroxenes from the Atlantis Bank and a negative correlation between Mg-values and Al_2O_3, TiO_2, and Na_2O (Figure 6). Clinopyroxenes within hybridized gabbros show lower Mg values but similar Al_2O_3, TiO_2, and Cr_2O_3 compositions to clinopyroxene in olivine gabbros (Mg# = 68.3–83.8 mol%; Al_2O_3 = 1.5–3.3 wt%; TiO_2 = 0.29–0.72 wt%; Cr_2O_3 = 0.01–0.27 wt%; Figure 6). Within the dolerite intrusion, clinopyroxenes show a large range of within-sample compositional variation, from primitive compositions within phenocrysts (Mg# = 81.0–85.7 mol%; Al_2O_3 = 2.75–3.43 wt%; TiO_2 = 0.44–0.63 wt%; Cr_2O_3 = 0.06–0.66 wt%) to more evolved compositions in the fine-grained matrix (Mg# = 69.7–81.6 mol%; Al_2O_3 = 1.27–5.31 wt%; TiO_2 = 0.47–1.30 wt%; Cr_2O_3 = 0.01–0.45 wt%).

Plagioclase (Figure 7) shows a large compositional range in the olivine gabbros, with higher anorthite contents in the fine-grained gabbro (An = 61.1–66.8 mol%; An = Ca/[Ca + Na + K]), progressively decreasing in varitextured (An = 57.9–66.9 mol%) and coarse-grained olivine gabbros (An = 51.6–67.3 mol%), while K_2O is rather low and constant in plagioclase from all the olivine gabbros (K_2O = 0.00–0.18 wt%; Figure 7a). Within varitextured gabbros, plagioclase in the gabbro patches shows slightly more anorthitic compositions (average An = 60.6 mol%) than their host gabbro (average An = 58.8 mol%; Table S4). Plagioclase in oxide gabbro shows more evolved compositions and a negative correlation between the anorthite content and K_2O concentration (An = 30.9–47.1 mol%, K_2O = 0.02–0.22 wt%; Figure 7a). In the dolerite intrusion, plagioclase shows primitive compositions in the phenocrysts (An = 68.1–68.4 mol%; K_2O = 0.02–0.04 wt%) and more evolved compositions in the fine-grained matrix (An = 55.0–64.1 mol%; K_2O = 0.04–0.11 wt%). Within the

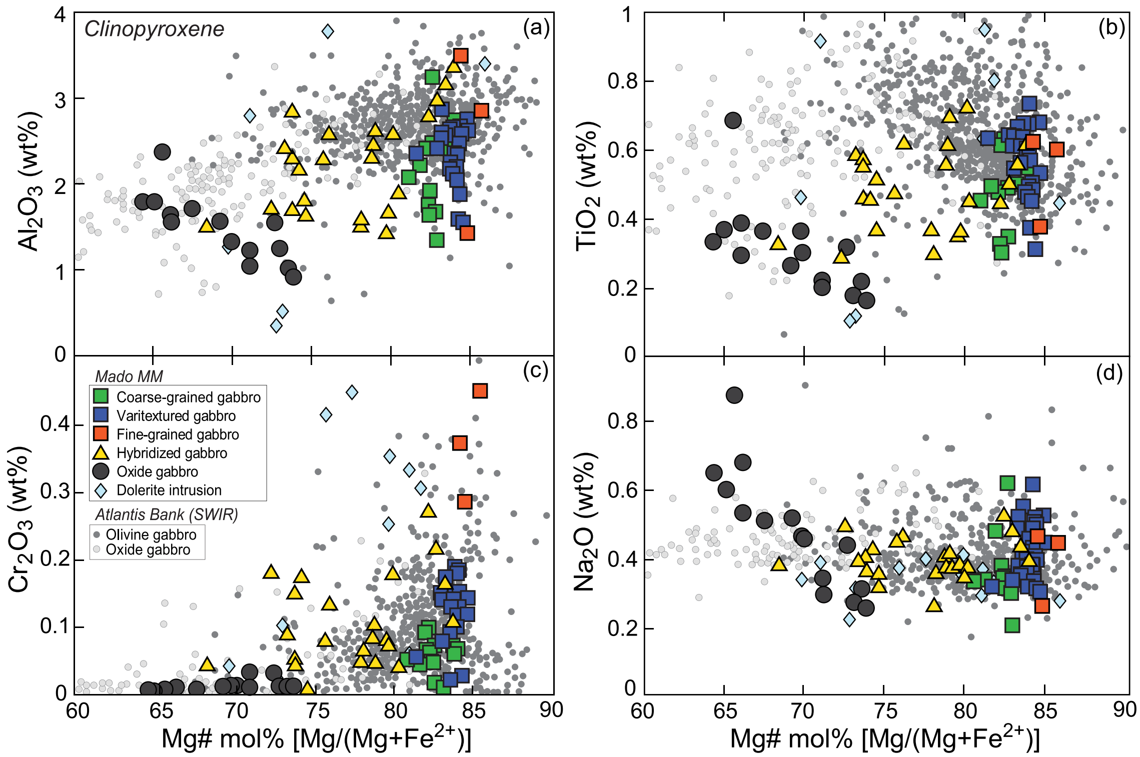

Figure 6. Mg value (Mg# = Mg/(Mg + Fe) mol%) against major element compositions of primary magmatic clinopyroxenes within the Mado Megamullion gabbroic crust. (a) Al_2O_3 (wt%); (b) TiO_2 (wt%); (c) Cr_2O_3 (wt%); (d) Na_2O (wt%). Major element compositions of olivine gabbros and oxide gabbros from Atlantis Bank (Southwest Indian Ridge; Dick et al., 2002; Nguyen et al., 2018) are shown for comparison.

felsic veins, plagioclase is characterized by evolved compositions, and a negative correlation is seen between anorthite content and K_2O concentration (An = 24.3–47.7 mol%; K_2O = 0.01–0.41 wt%; Figure 7b). Figure 8 shows sodium EDX qualitative mapping of the different occurrences of felsic veins. The straight contact (Figure 5a) between the sharp felsic vein and its host coarse-grained olivine gabbro is accompanied by a sharp chemical boundary (Figure 8a). The diffuse felsic vein is characterized by a reaction zone (Figure 5b) and a diffuse chemical boundary showing progressive Na decrease in plagioclase from the felsic vein (An = 38 mol%) to the partially re-equilibrated fine-grained gabbro (An = 62 mol%; Figure 8b). The hybridized gabbro lenses enclosed within the diffuse felsic veins show the largest compositional range of all lithotypes (Figure 7a; An = 24.3–61.6 mol%; K_2O = 0.01–0.41 wt%); in places they preserve the composition of the preexisting gabbro (An = 58 mol%; Figure 8c) but are otherwise re-equilibrated and show evolved compositions, similar to the felsic veins. Taken as a whole, the felsic material within the Mado Megamullion gabbroic crust shows similar compositions to plagioclase analyzed in diffuse, reactive, and sharp veins from Atlantis Bank (Figure 7b; Nguyen et al., 2018).

The plagioclase anorthite and clinopyroxene Mg-value covariation defines a positive correlation (Figure 7c) that follows the slope of the trend defined by the gabbros in the Godzilla Megamullion (Harigane et al., 2011; Sanfilippo et al., 2013, 2016). Notably, the Mado Megamullion gabbroic crust defines a trend characterized by relatively low anorthite contents (Figure 7c), similar to what was documented in the Godzilla Megamullion lower crust (Sanfilippo et al., 2016). On the other hand, the dolerite intrusion plots outside the trend defined by the gabbros, at higher anorthite values (Figure 7c).

Amphibole in the Mado Megamullion occurs as brown, dark green, and pale green amphibole (Figures 4 and 5). We distinguished different occurrences of amphibole on the basis of their microstructural relationships within the different lithotypes, namely, (i) brown magmatic amphibole that is found ubiquitously in the gabbros; (ii) brown amphibole in granulite-facies mylonitic bands; (iii) brown to dark-green amphibole in amphibolite-facies mylonitic bands; (iv) dark-green magmatic amphibole within the felsic veins; (v) dark-green amphibole in crosscutting amphibole-rich veins; and (vi) pale-green amphibole associated

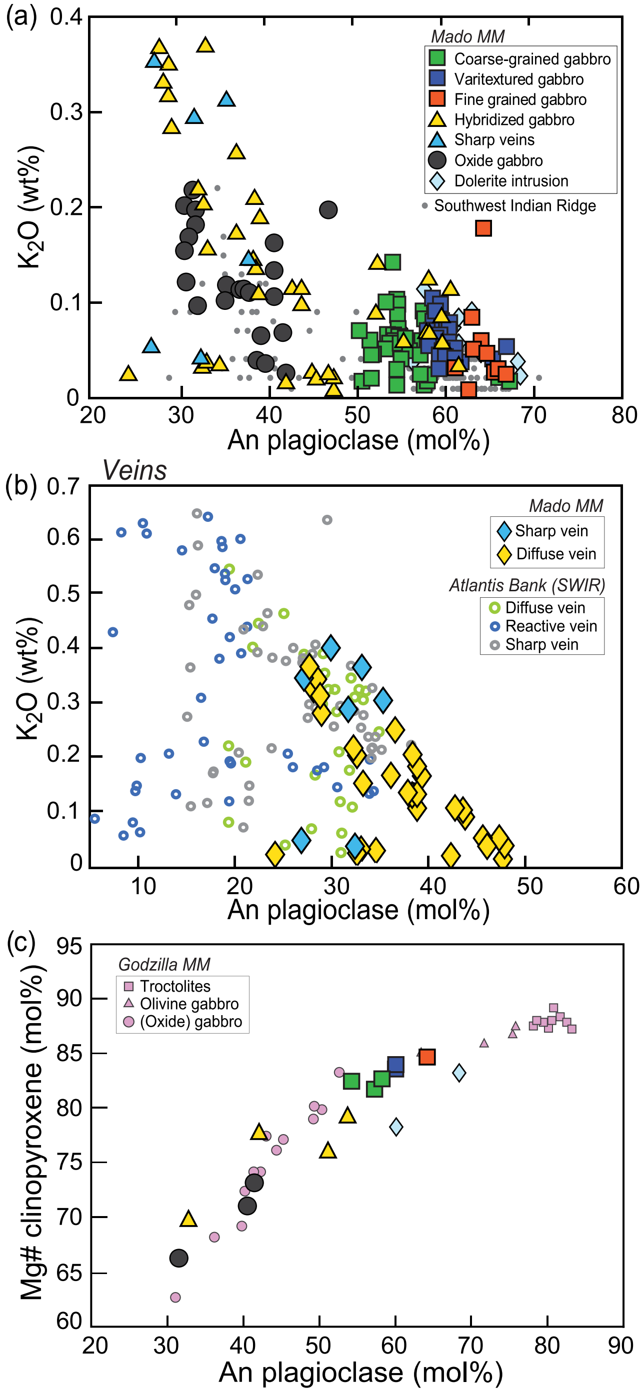

Figure 7. Major element compositions of primary magmatic plagioclases within the Mado Megamullion gabbroic crust. (a) Anorthite versus K_2O (wt%) of all studied lithotypes. Plagioclase compositions from the Atlantis Bank (Southwest Indian Ridge, IODP Hole 735B: Dick et al., 2002) are shown for comparison; (b) anorthite versus K_2O (wt%) of the felsic veins crosscutting the Mado Megamullion gabbroic crust. Plagioclase compositions of felsic veins from Atlantis Bank (Southwest Indian Ridge; Nguyen et al., 2018) are reported for comparison; (c) covariation trend of Mg# in clinopyroxene and Anorthite contents in plagioclase. Compositions of clinopyroxenes and plagioclases from the Godzilla Megamullion troctolites and gabbros (Sanfilippo et al., 2013, 2016) are shown for comparison.

with low-temperature alteration of clinopyroxene. Magmatic amphiboles are found within all gabbros, from olivine gabbros to oxide gabbros, and show pargasitic to edenitic compositions (amphibole classification after Leake et al., 1997), characterized by Si-poor and Na + K-, TiO_2-, and Al-rich compositions (Si a.p.f.u. = 6.31–6.98; Na + K a.p.f.u. = 0.47–0.89; TiO_2 = 1.95–3.58 wt%; Al a.p.f.u. = 1.01–1.68; Figure 9). Amphiboles within the granulite-facies mylonite (Si a.p.f.u. = 6.46–6.57; Na + K a.p.f.u. = 0.61–0.72; TiO_2 = 1.47–2.95 wt%; Al a.p.f.u. = 1.43–1.54; Figure 9) and amphibolite-facies mylonite (Si a.p.f.u. = 6.48–7.00; Na + K a.p.f.u. = 0.47–0.74; TiO_2 = 1.24–2.22 wt%; Al a.p.f.u. = 0.99–1.52; Figure 9) show similar compositions to the magmatic amphiboles. Within the felsic veins and amphibole-rich veins, amphiboles are edenite to hornblende, showing lower Na + K, Al, and TiO_2 and higher Si concentrations (felsic vein: Si a.p.f.u. = 6.63–7.18; Na + K a.p.f.u. = 0.39–0.73; TiO_2 = 0.45–2.00 wt%; Al a.p.f.u. = 0.82–1.37; amphibole-rich vein: Si a.p.f.u. = 6.61–7.31; Na + K a.p.f.u. = 0.35–0.69; TiO_2 = 0.34–1.33 wt%; Al a.p.f.u. = 0.69–1.39; Figure 9). Low-temperature amphibole alteration of clinopyroxene shows tremolitic to hornblende composition characterized by Si-rich and Na + K-, TiO_2-, and Al-poor compositions (Si a.p.f.u. = 6.57–7.98; Na + K a.p.f.u. = 0.01–0.51; TiO_2 = 0.01–0.88 wt%; Al a.p.f.u. = 0.02–1.43; Figure 9).

6.2. Amphibole-Plagioclase Geothermometry

Amphibole-plagioclase equilibrium temperatures, representative of crystallization and mylonitic deformation recorded in the Mado Megamullion lower gabbroic crust were obtained by using the plagioclase-amphibole geothermometer from Holland and Blundy (1994), at pressures ranging from 0.5 to 2 kbar. The latter were obtained using the plagioclase-amphibole geobarometer from Anderson and Smith (1995). These plagioclase-amphibole equilibrium temperatures were compared with the results of single-amphibole geothermometers, namely, Ti in amphibole (Otten, 1984) and Si-Ti-Fe-Na in amphibole (Putirka, 2016; Ridolfi & Renzulli, 2011). The temperature estimates obtained are representative of (i) magmatic crystallization; (ii) granulite-facies mylonitic recrystallization; (iii) amphibolite-facies mylonitic recrystallization; (iv) formation of felsic veins; (v) formation of crosscutting amphibole-rich veins; and (vi) low-temperature alteration. The three geothermometers yield comparable results, which are represented in Figure 10 (see also Table S6), which show a decrease in average temperature registered from magmatic crystallization in the gabbros (955–881°C) to granulite-facies mylonite (929–871°C), amphibolite-facies mylonite (847–807°C), formation of the felsic veins (847–793°C), formation of amphibole-rich veins (842–741°C), and a diffuse amphibolitization associated to the formation of tremolite and hornblende (686–622°C).

6.3. Basalt Whole-Rock Compositions

The two basalts recovered at the Mado Megamullion (Table S1) are characterized by rather evolved Mg-values (Mg# = 40.34–42.66 mol%) and Ca-numbers (Ca# = 63.74–66.79 mol%; Ca# = Ca/[Ca + Na + K]). They show flat M-HREE patterns (Yb_N = 1.14–1.32 times N-NORB; Figure 11) and selective enrichments in the most incompatible LREE (La_N = 3.57–4.07 times N-MORB; Figure 11) and fluid-mobile trace elements (Rb, Ba, Th, U, K, La, Ce, Pb, Sr; Figure 11) relative to basalts from the Southwest Indian Ridge (Coogan et al., 2004), Mid-Atlantic Ridge (Gale et al., 2013),

10.1029/2020GC009199

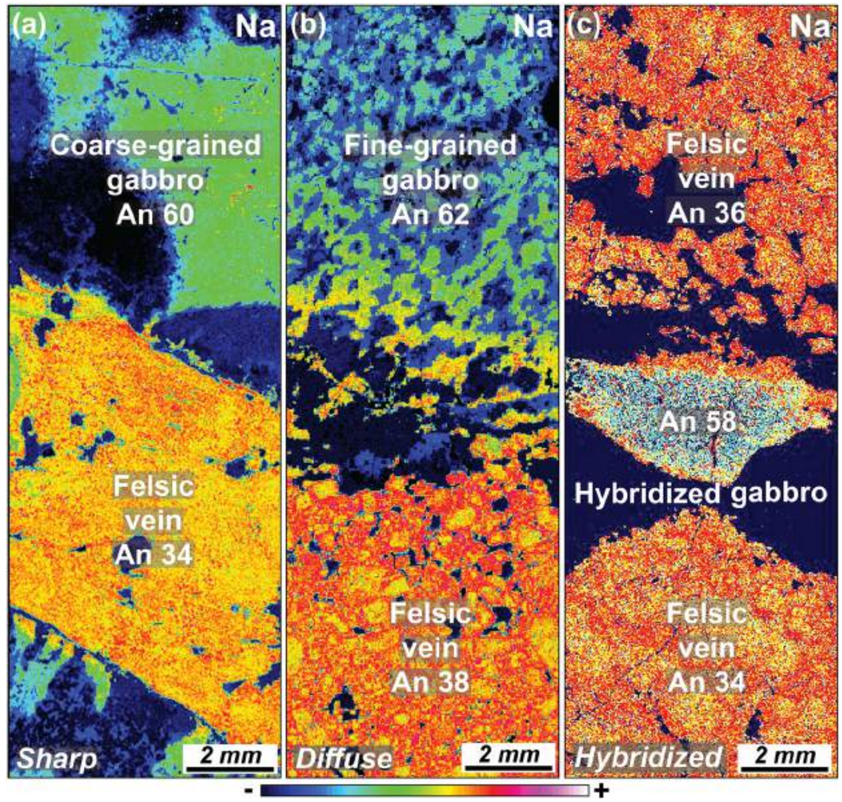

Figure 8. EDX Na mapping of the different occurrences of felsic veins. (a) Sharp contact with host gabbro; (b) diffuse contact with host gabbro; (c) hybridized gabbro included within a diffuse felsic vein. "An" refers to the representative plagioclase Anorthite content.

and East Pacific Rise (Zhang et al., 2018). The compositions of the Mado Megamullion basalts are generally similar to the compositions documented in coeval basalts from the central Shikoku Basin (Ishizuka et al., 2009).

7. Discussion

The Mado Megamullion is a topographic high located at an inside corner of a ridge-transform-ridge intersection in the extinct Shikoku Basin (Figure 1b). It presents the typical morphological features of an OCC (Escartìn et al., 2017, and references therein), that is, (i) domal surface showing spreading-parallel corrugations; (ii) a breakaway and a termination area (Figure 2b); (iii) positive mantle Bouguer anomalies (Ohara et al., 2018; Okino et al., 2019); and (iv) exposure of gabbros and mantle peridotites (Figure 2c; Table 1). The corrugated surface is ~500 km^2 (Figure 1b), similar in size to most OCCs documented at the Mid-Atlantic Ridge and Southwest Indian Ridge. These morphological and compositional features confirm the presence of OCCs in the Shikoku Basin, as previously inferred by the Japan's continental shelf survey (e.g., Ohara et al., 2015). Similar to the Godzilla Megamullion in the Parece Vela Basin, the formation of the Mado Megamullion occurred during the last phases of spreading of an extinct back-arc basin, most likely in a period of slow spreading. In the following, we discuss the tectono-magmatic evolution of the lower oceanic crust exposed at the Mado Megamullion OCC, along with its compositional differences with representative gabbroic sections from the Pacific, Atlantic, and Indian oceans.

7.1. Chemical Evolution of the Lower Crust at Mado Megamullion

The gabbroic crust exposed on the corrugated surface of the Mado Megamullion is mainly formed of olivine gabbros ranging from coarse to fine grained and from granular to varitextured (Figures 2a and 2b). The variability in texture of the undeformed samples is also mirrored by rather distinct compositions of clinopyroxene (Figure 6) and plagioclase (Figure 7a), which are slightly more primitive in fine-grained olivine gabbros compared to the varitextured and coarse-grained olivine gabbros.

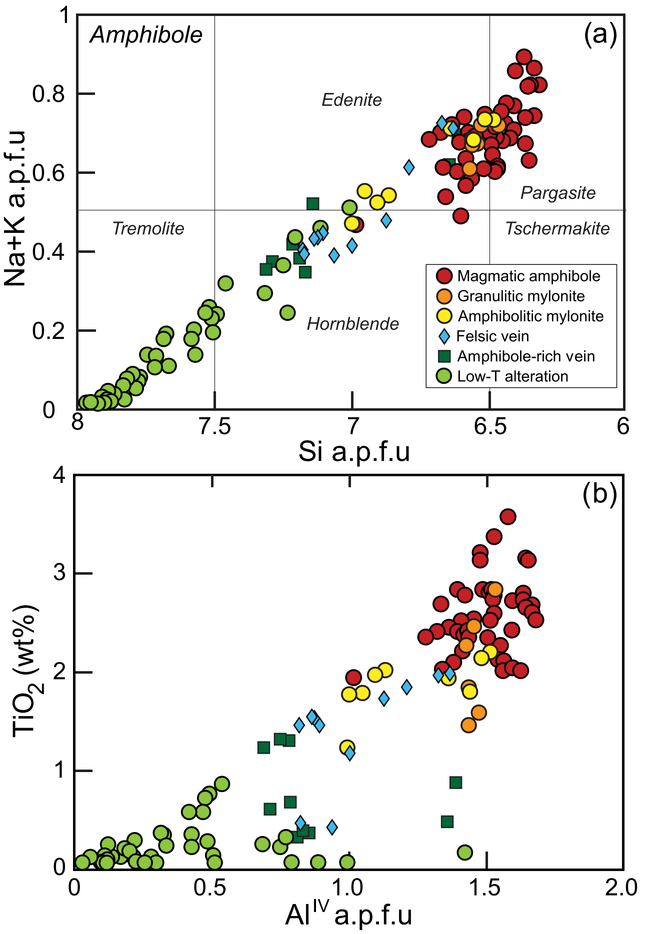

Figure 9. Amphibole major element compositions within the Mado Megamullion gabbroic crust. Amphiboles were subdivided according to their microstructural relationship, regardless of the lithology. Magmatic amphiboles are found in all gabbro types, from olivine gabbro to oxide gabbro. (a) Si a.p.f.u. (atom per formula unit) versus [Na + K] a.p.f.u. amphibole classification after Leake et al. (1997); (c) Al^{IV} a.p.f.u. versus TiO_2 (wt%).

Varitextured olivine gabbros are characterized by the occurrence of millimeter-size rounded patches of fine-grained plagioclase and pyroxene (Figures 4c and 4d) enclosed within a coarse-grained gabbro. The patches are also characterized by high amounts of Ti-pargasite (10–15 vol%) and slightly higher plagioclase anorthite contents (average An = 60.6 mol%) compared to the host coarse-grained gabbro (average An = 58.8 mol%; Table S4). Experimental investigations demonstrated that elevated water contents in MORB melts favor the saturation of clinopyroxene over plagioclase and lead to early saturation of amphibole and to the crystallization of anorthitic plagioclase (Berndt et al., 2005; Koepke et al., 2009). Accordingly, we interpret the millimeter-size patches to be crystallized from a melt relatively enriched in water compared to that forming the coarse-grained gabbros. Similar fine-grained patches have been previously described at the East Pacific Rise (IODP Hole 1256D; Koepke et al., 2011) and the Oman Ophiolite (France et al., 2009). In the latter, varitextured gabbros are generally located at the gabbro-dike transition and interpreted as the crystallization of residual melt trapped in "pockets" during a process of in situ crystallization of the peripheral portions of axial melt lenses. The millimeter-size rounded patches from the Mado Megamullion are also consistent with this interpretation. However, the varitextured gabbros at dike-gabbro transition from fast spreading ridges are saturated in oxides and have highly evolved compositions (see Koepke et al., 2011) consistent with a formation in axial melt lenses, whereas the varitextured gabbros from the Mado Megamullion have a relatively primitive composition and cannot be assumed to be "frozen melts." More likely, these varitextured gabbros formed by a localized process of in situ crystallization of melt droplets during near-solidus crystallization of the olivine gabbro at depth and at relatively low temperatures ($T = 918–959°C$; Table S6). This is consistent with the extensive cooling expected in these environments as a consequence either of the scarcity of melt supply or exhumation through detachment faulting (e.g., Coogan et al., 2007; Ferrando et al., 2020).

Oxide gabbros are exclusively sampled at the transform wall (Figures 2a and 2b), where most of these rocks have been strongly affected by high-temperature shearing. They show a range of variation of Mg-value in clinopyroxene (Figure 6) and plagioclase anorthite contents (Figure 7a) similar to oxide gabbros documented at the Atlantis Bank (Dick et al., 2002). Plagioclase shows positive correlation between anorthite content and K_2O (Figure 7a), and the Mg#$_{cpx}$-Anorthite$_{plg}$ covariation trend defines a continuous evolution from olivine gabbros to oxide gabbros, at low Anorthite contents (Figure 7c). These features suggest that oxide gabbros at the Mado Megamullion formed from the melts that previously fractionated to form the olivine gabbros. The formation of oxide gabbros from ferrobasaltic melts, as part of the MORB differentiation trend, has been previously documented in experimental studies (Botcharnikov et al., 2008; Koepke et al., 2018) and in the Atlantis Bank gabbroic crust (Dick et al., 2000, 2002; Dick, MacLeod, et al., 2019; MacLeod et al., 2017; Natland & Dick, 2002).

As a whole, the oxide gabbros of the Mado Megamullion are compositionally similar to those from the Atlantis Bank core complex (Dick et al., 2002). However, a closer inspection reveals that there are substantial differences between the two sample suites. Clinopyroxenes from the Mado Megamullion oxide gabbros have low TiO_2 and Al_2O_3 contents and negative correlations between Mg value and Al_2O_3, TiO_2, and Na_2O (Figure 6), whereas in the Atlantis Bank oxide gabbros both Al_2O_3 and TiO_2 decrease at decreasing Mg value in clinopyroxene, as result of saturation in Fe-Ti oxides (Dick et al., 2002; Koepke et al., 2018), but Na_2O remains constant (Figure 6). This marked difference in the crystal line of descent may indicate a quite different compositional evolution of the magmas during magmatic differentiation in the Mado Megamullion OCC compared to the Atlantis Bank. Also, in the Mado Megamullion, oxide gabbros are rich in amphibole (up to

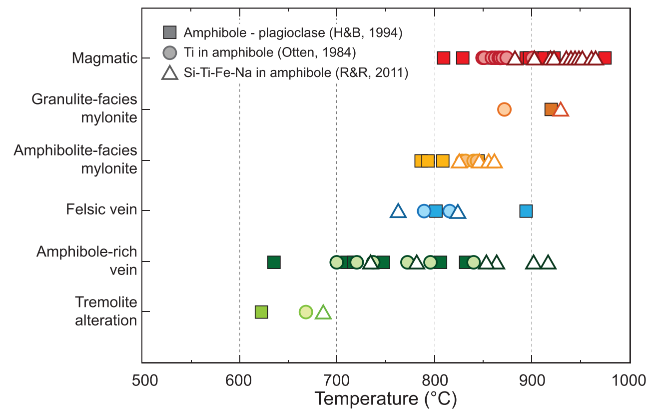

Figure 10. Temperature estimates calculated using the edenite-richterite amphibole-plagioclase geothermometer (Holland & Blundy, 1994), at pressures calculated by iteration for the corresponding compositions (Anderson & Smith, 1995). The resulting temperature estimates are compared to the Ti-in-amphibole geothermometer (Otten, 1984) and the Si-Ti-Fe-Na-in-amphibole geothermometer (Ridolfi & Renzulli, 2011).

10 vol%; Figure 5d), which is only a minor phase in the Atlantis Bank oxide gabbros where it occurs as trace amounts (1–5 vol%) (see also MacLeod et al., 2017). Ti-pargasite is also ubiquitous as a granular to interstitial magmatic phase within the olivine gabbros from the Mado Megamullion, where it locally exceeds 5 vol% in the primitive fine-grained lithologies (Figure 4b). At the same time, Ti-pargasite is also widespread in gabbros from the Godzilla Megamullion (Harigane et al., 2011, 2019; Sanfilippo et al., 2013, 2016), and from the Central Graben of the Mariana Trough (Bloomer et al., 1995; Ohara et al., 2002; Stern et al., 1997), an intraoceanic rift related to back-arc spreading (Ohara et al., 2002). Therefore, the abundance of magmatic amphibole from primitive to evolved lithologies could be a typical feature of the lower gabbroic crust at back-arc environments, likely related to a hydrous character of the parental melts. Indeed, experiments have shown that high water activity in basaltic melt allows the early saturation of Ti-pargasite amphibole at temperatures as high as 950°C (Botcharnikov et al., 2008; Feig et al., 2006; Koepke et al., 2018), consistent with the amphibole crystallization temperatures that we documented in the Mado Megamullion gabbros (average $T_{amph\text{-}plg}$ = 881–955°C; Figure 10; Table S6). A water-saturated parental melt for the Mado Megamullion gabbroic crust is also consistent with enrichments in fluid-mobile trace elements (Rb, Ba, Th, U, K, La, Ce, Pb, and Sr), compared to typical MORB compositions. These are documented in the basalts from the Shikoku Basin and Mado Megamullion (Figure 11; Table S1). The fluid-mobile element enrichments require a subduction fluid component in the mantle source of these melts (Kessel et al., 2005; Shervais & Jean, 2012), consistent with a back-arc environment (Ohara et al., 2018; Okino et al., 2019). Therefore, we infer that the olivine and oxide gabbros from the Mado Megamullion most likely experienced early crystallization of amphibole as a product of primary melts slightly enriched in water relative to N-MORB. Elevated water activity (Botcharnikov et al., 2008; Sisson & Grove, 1993) and oxygen fugacity in the melt might also have caused the early saturation of Fe-Ti oxides (Berndt et al., 2005; Botcharnikov et al., 2008; Toplis & Carroll, 1995). The coupled effect of amphibole-Fe-Ti oxide crystallization would lead to a significant decrease in the TiO_2 and Al_2O_3 contents of the residual melts, also buffering the melts toward low water activity (Berndt et al., 2005; Feig et al., 2006; Husen et al., 2016; Koepke et al., 2009); this could in turn explain the low TiO_2 and Al_2O_3 contents of clinopyroxene in the Mado Megamullion gabbros compared to those of the Atlantis Bank (Figure 6). We postulate that the crystallization of the evolved gabbros in this study occurred from melts depleted in Ti and Al after early crystallization of Ti-pargasite and Fe-Ti oxides. It is worth noting that our results are in agreement with recent studies focused on the liquid lines of descent of hydrous MORB, which are characterized by low TiO_2 and CaO/Al_2O_3, and high Na_2O and SiO_2 contents as a consequence of delayed plagioclase saturation together with early crystallization of clinopyroxene and Fe-Ti oxides (Botcharnikov et al., 2008; Husen et al., 2016; MacLeod et al., 2013). This is consistent with mineral compositions in the Mado Megamullion evolved gabbros, where high Na_2O and low TiO_2 and Al_2O_3 in clinopyroxene (Figure 6) coexist with low anorthite contents in plagioclase (Figure 7a). We will hereafter discuss whether this process may explain the distinctive crystal line of descent of other gabbro occurrences from the Philippine Sea back-arc basin compared to typical mid-ocean ridge sections.

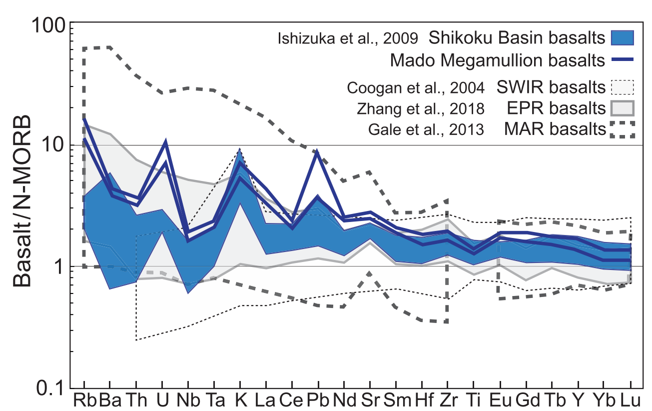

Figure 11. Basalt trace element compositions from the Shikoku Basin (Ishizuka et al., 2009) and Mado Megamullion (this study), compared to the Southwest Indian Ridge (Coogan et al., 2004), East Pacific Rise (Zhang et al., 2018), and Mid-Atlantic Ridge (Gale et al., 2013). The trace element patterns are normalized to N-MORB composition (Workman & Hart, 2005).

7.2. Distinctive Composition of the Lower Crust at the Mado Megamullion: Evidence for Chemical Differentiation in Back-Arc Environments?

Figure 12 shows the plagioclase anorthite versus clinopyroxene Mg-value covariation for the gabbros at the Mado Megamullion compared to two other lower crustal sections from the Parece Vela Basin and Mariana Trough. These are compared to three archetypical sections from

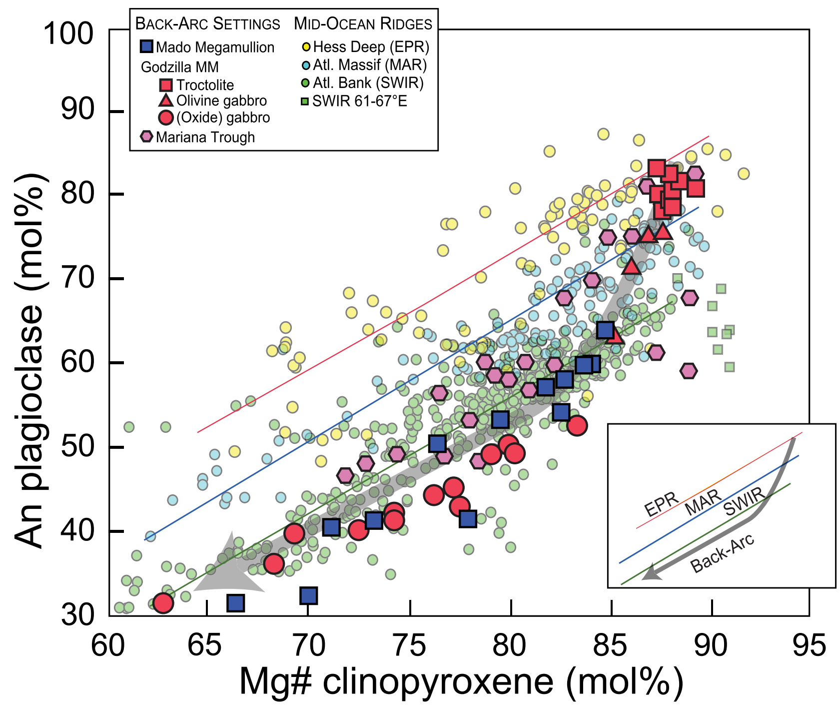

Figure 12. Variations of Mg# in clinopyroxene versus Anorthite in coexisting plagioclase from gabbros formed in the Philippine sea back-arc basins—Mado Megamullion (this study); Godzilla Megamullion (Harigane et al., 2008, 2010, 2011; Sanfilippo et al., 2013, 2016); Mariana Trough (Ohara et al., 2002)—compared to those from mid-ocean ridges gabbroic rocks from Hess Deep at East Pacific Rise (Dick & Natland, 1996; Lissenberg et al., 2013), Atlantis Bank at Southwest Indian Ridge (Dick et al., 2002), and Atlantis Massif at Mid-Atlantic Ridge (Drouin et al., 2009; Ferrando et al., 2018; Miller et al., 2009; Suhr et al., 2008). The regression lines for the three lower crustal sections are calculated and reported in the plot. Note that gabbroic rocks from the Godzilla Megamullion, Mariana Through, and Mado Megamullion follow a distinct fractionation trend that at high Cpx Mg# crosscut those of the three MOR sections. All samples from these settings except the primitive troctolites from the Godzilla Megamullion are amphibole-bearing.

mid-ocean ridges (East Pacific Rise, Mid-Atlantic Ridge, and Southwest Indian Ridge). At mid-ocean ridges, these covariation trends are characterized by different anorthite contents and by a constant slope from primitive to evolved lithotypes. The shift in anorthite content between the different sections is typically related to the overall Na contents of the primitive melts, being in turn mostly related to different degrees of mantle melting (Basch, Rampone, Borghini, et al., 2019; Dick et al., 1984; Kempton & Casey, 1997; Klein & Langmuir, 1987; Sanfilippo et al., 2013).

Different from what is depicted in "mid-ocean ridge" settings, Sanfilippo et al. (2013, 2016) noted that the gabbros from the Godzilla Megamullion define a distinctive crystal line of descent, which at high clinopyroxene Mg value produce a steep trend evolving from highly anorthitic plagioclase in troctolites to rather albitic plagioclase in olivine gabbros (see also Basch, Rampone, Crispini, et al., 2019). At more evolved compositions (i.e., from olivine to oxide gabbros) the Godzilla Megamullion gabbros follow the trend defined by the mid-ocean ridge gabbros, plotting in the field of the gabbros from Atlantis Bank, at relatively low anorthite contents (Figure 12). A similar trend is also defined by the gabbros from the Mariana Trough (Bloomer et al., 1995; Ohara et al., 2002; Stern et al., 1996). The steep trend at primitive compositions was explained at the Godzilla Megamullion by early crystallization of clinopyroxene, which might have lowered the CaO/(CaO + Na_2O) ratio in the residual melt (Sanfilippo et al., 2016). Early saturation of clinopyroxene can be interpreted either as the result of partial assimilation of the lithospheric mantle (see also Basch, Rampone, Borghini, et al., 2019; Collier & Kelemen, 2010) or from high water activity delaying plagioclase saturation (Berndt et al., 2005; Botcharnikov et al., 2008; Feig et al., 2006; Husen et al., 2016; Koepke et al., 2009). Highly primitive lithologies, such as troctolites and wehrlites, have not been sampled at the Mado Megamullion, but the compositions of olivine gabbros and oxide gabbros are nearly identical with those of the other two back-arc sequences. In addition, in the previous section we showed that the

10.1029/2020GC009199

composition of the gabbroic crust from the Mado Megamullion requires relatively high water contents in the parental melts to explain the high amount of Ti-pargasite, and the relatively low Ti and Al and high Na contents in clinopyroxene coupled with low anorthite in coexisting plagioclase. Enriched compositions of the Shikoku Basin basalts further support a parental melt composition bearing subduction fluid components. On these bases, we here infer that the "anomalous" crystal lines of descent of the gabbros from the Mado Megamullion, Godzilla Megamullion, and Mariana Trough can be typical of back-arc basins.

We infer that the water-rich character of the primary melt produced in back-arc basins causes a chemical evolution of the lower crust markedly different compared to that of the "dry" melts at mid-ocean ridges. Although the primitive lithologies have high anorthite contents in plagioclase as a consequence of the elevated water activity, the early precipitation of abundant clinopyroxene leads to a decrease in the melt $CaO/(CaO + Na_2O)$ ratio. High water activity also causes early saturation of Fe-Ti oxides and Ti-pargasite, in turn leading to a strong decrease in Al, Ti, and water in the residual melt during the differentiation and to the crystallization of An-poor plagioclase in the evolved gabbros (Figure 12).

Current versions of the MELTS thermodynamic program (Ghiorso et al., 2002; Gualda et al., 2012) did not produce early saturation of magmatic amphibole, even at high water contents, and thus could not be used to quantitatively reproduce the distinct crystal line of descent envisaged in this study. However, we emphasize that the crystallization of magmatic amphibole at temperatures as high as 1,000°C has indeed been documented in experimental studies (e.g., Berndt et al., 2005; Botcharnikov et al., 2008; Feig et al., 2006; Koepke et al., 2011). Moreover, incorporation of water within the primary melt drastically decreases its liquidus temperature by delaying the saturation of silicates (e.g., Berndt et al., 2005; Botcharnikov et al., 2008; Feig et al., 2006). As a result, the crystallization of magmatic amphibole is expected at an early stage of melt fractionation, in turn explaining its ubiquitous presence as a primary magmatic phase.

Interestingly, mineral compositions in the late dolerite intrusion at the Mado Megamullion (both phenocrysts and fine-grained ophitic matrix) show higher anorthite contents in plagioclase at given clinopyroxene Mg-value compared to the plagioclase-clinopyroxene couples within the gabbroic crust (+10 mol% anorthite; Figure 7c). This suggests that these melts preserved high $CaO/(CaO + Na_2O)$ ratio similar to those of the parental melts and therefore did not experience fractionation within the lower crust but rather crystallized rapidly as doleritic dikes at nearly eutectic conditions. The preservation of high anorthite in plagioclase from the dolerites further supports the idea that the gradual decrease in anorthite seen in the gabbros is triggered by fractionation at lower crustal levels, rather than a primary feature.

7.3. Early Deformation History

Most of the studied olivine gabbros and oxide gabbros show evidence of crystal-plastic deformation (Figure 3b). At the Mado Megamullion, olivine gabbros show two different types of mylonitic recrystallization, characterized by plagioclase neoblasts associated with (i) clinopyroxene neoblasts with minor Ti-pargasite formed at granulite-facies conditions (Figures 4e and 4f) and (ii) edenitic amphibole ± Fe-Ti oxides formed at amphibolite-facies conditions (Figure 4g). Oxide gabbros only present amphibolite-facies mylonitic recrystallization of clinopyroxene porphyroclasts. Granulite-facies mylonitic shear zones are widespread at modern OCCs—Godzilla Megamullion (Harigane et al., 2008, 2010, 2011, 2019; Michibayashi et al., 2016), Mid-Atlantic Ridge (Blackman et al., 2006, 2011; Coogan et al., 2001; Dick et al., 2008; Hansen et al., 2013; Sanfilippo et al., 2018; Schroeder & John, 2004), and Southwest Indian Ridge (Dick et al., 2000; Dick, Kvassnes, et al., 2019; Dick, MacLeod, et al., 2019; MacLeod et al., 2017; Mehl & Hirth, 2008; Miranda & John, 2010)—and in other fossil examples of OCC such as in the Alpine ophiolites (e.g., Sanfilippo & Tribuzio, 2011; Tribuzio et al., 2020). They were interpreted as the early expression of a growing detachment fault and formed at temperatures as high as 1,000°C (e.g., Mehl & Hirth, 2008; Sanfilippo et al., 2018). Amphibolite-facies mylonitic recrystallization is a much less common feature at OCCs in the mid-ocean ridge lithosphere and has so far been documented only at the Atlantis Bank (Dick et al., 2000; MacLeod et al., 2017). On the other hand, amphibolitic mylonites are common at Godzilla Megamullion (Harigane et al., 2008, 2010, 2011, 2019) and in some sections of the Alpine ophiolites (Sanfilippo & Tribuzio, 2011; Tribuzio et al., 2020).

At the Mado Megamullion, the recrystallized Ti-pargasite found in mylonitic aggregates is nearly indistinguishable in composition from the magmatic Ti-pargasite in undeformed samples (Figure 9).

10.1029/2020GC009199

Granulite-facies and amphibolite-facies mylonitic aggregates yield consistent high recrystallization temperatures of 929–871°C and 847–807°C, respectively (Figure 10; after Holland & Blundy, 1994; Otten, 1984; Ridolfi & Renzulli, 2011). These temperature estimates plot within the range already documented for granulite-grade deformation in the Atlantis Bank gabbroic crust (946 ± 70°C; Mehl & Hirth, 2008; Miranda & John, 2010) and at 16.5°N Mid-Atlantic Ridge OCC (1,010–930°C; Sanfilippo et al., 2018). The high temperatures of deformation and recrystallization are similar to the experimentally determined upper temperature limit for amphibole stability (Botcharnikov et al., 2008; Koepke et al., 2004, 2007) and higher than solidus temperature of a hydrous MORB melt (800–900°C; Botcharnikov et al., 2008; Koepke et al., 2018). This suggests that deformation could have initiated at hypersolidus conditions, that is, in the presence of some small fractions of melt. This is sustained by the local occurrence of Ti-pargasite with interstitial to poikilitic textures within the neoblastic assemblages. The complex interplay between high-temperature mylonitic deformation and melt percolation and crystallization has been previously numerically modeled (Tucholke et al., 2008) and is typical of many OCCs worldwide including the Atlantis Bank (see Dick, MacLeod, et al., 2019; MacLeod et al., 2017), the Godzilla Megamullion (Harigane et al., 2019), and at the Mid-Atlantic Ridge (Agar & Lloyd, 1997; Sanfilippo et al., 2018). At the Mado Megamullion, the ubiquity of magmatic amphibole in the undeformed lithotypes implies that the formation of Ti-pargasite during the granulite-facies event did not require external water entering into the deforming gabbros. On the other hand, amphibolite-facies mylonites likely involved some input of seawater-derived fluids during deformation, but still at high temperature conditions (Figure 10). The flux of hydrothermal water into the detachment fault (e.g., Harigane et al., 2008; Miranda & John, 2010) and a possible role of magmatic amphibole in controlling the rheology of the lower gabbroic crust at back-arc basins (e.g., Harigane et al., 2019) will be tested in future studies focused on the conditions of emplacement of the mylonitic gabbros.

We conclude that the crystal-plastic deformation of the lower crust at the Mado Megamullion records progressive exhumation of a crustal gabbroic sequence from hypersolidus conditions in a crystallizing magmatic body to shallower conditions under the influence of hydrothermal fluids, as a consequence of a long-lived system of detachment faults (Figure 13a). Extensive hydrothermal activity is further confirmed by the recovery of a rodingite sample on the detachment surface during dredge KH07-2-D28 (Ohara et al., 2018).

7.4. Intrusion of Felsic Veins and Progressive Exhumation

The Mado Megamullion olivine gabbros are widely crosscut by felsic veins showing diffuse to sharp contacts with the host gabbro. These felsic veins are formed of albitic plagioclase (Figure 7b) and interstitial amphibole ranging from edenitic to hornblende in composition (Figure 9). Most occurrences of felsic veins show diffuse contacts marked by a millimeter-thick amphibole + Fe-Ti oxides + apatite reaction zone (Figure 5b). These reaction zones are coupled with diffuse chemical contacts in the host rock showing plagioclases progressively enriched in albite content approaching the felsic vein (Figure 8b). This suggests a progressive re-equilibration of the minerals in the host rock with the melt crystallizing the felsic material. In places, the intrusion of felsic material disrupted the preexisting gabbroic framework, enclosing millimeter-size portions of host olivine gabbros during emplacement (i.e., hybridized gabbro; Figure 3a). These hybridized rocks preserve textural and chemical characteristics of the preexisting olivine gabbro, thus clearly indicating a relict origin (Figure 8c). For instance, the re-equilibration of the preexisting minerals with the invading melt leads to a decrease in plagioclase anorthite contents (Figure 7a), and Mg value in clinopyroxene, while preserving the primary TiO_2, Cr_2O_3, Al_2O_3, and Na_2O concentrations (Figure 6). These chemical features indicate that the emplacement of the diffuse felsic veins occurred at rather high temperatures, allowing for reaction between the felsic melt and the host rock. Nonetheless, the host rocks and hybridized gabbros still preserve evidence for crystal-plastic deformation, whereas the albitic plagioclase is nearly undeformed. This suggests that the percolation of the felsic melts postdated the high-temperature deformation (Figure 13b). These observations confine the upper temperature of emplacement of the felsic material that, based on amphibole-plagioclase geothermometry, indicate a maximum crystallization temperature of 793–847°C (Figure 10), slightly lower than the granulite-facies deformation event in the host rock (871–929°C; Figure 10). On the other hand, the intrusion of felsic melts also occurred at lower temperature conditions, as indicated by the occurrence of sharp felsic veins at the contact between two gabbros showing different deformation intensities, most likely representing a brittle discontinuity involving displacement of the host rock (Figures 3b and 5a). The intrusion of felsic material therefore occurred at temperature

10.1029/2020GC009199

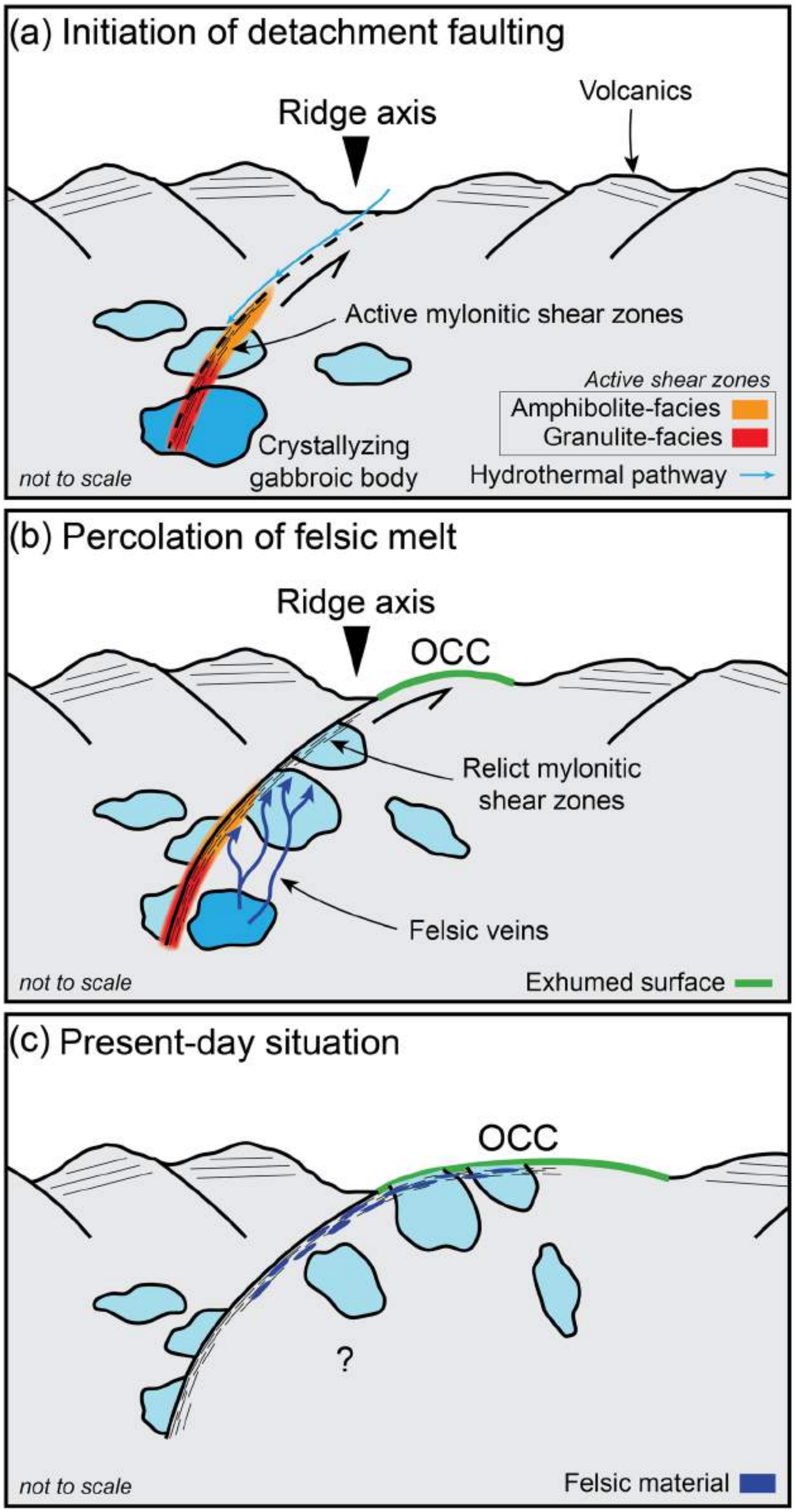

Figure 13. Sketch representing the formation and exhumation evolution of the Mado Megamullion oceanic lithosphere. (a) Deep-seated formation of the host gabbros and initiation of the detachment fault. Formation of active mylonitic shear zones at depth (red and yellow color); (b) percolation of felsic veins within the host gabbros and relict mylonitic shear zones during progressive exhumation of the OCC; (c) present-day situation, that is, exhumed gabbroic body, partially deformed in mylonitic shear zones and percolated by felsic veins.

10.1029/2020GC009199

conditions ranging from near-solidus (diffuse felsic veins) to brittle (sharp felsic veins) implying the percolation of this material along the detachment fault during the entire exhumation history (Figure 13b). Similar conditions have been documented in the Atlantis Bank gabbros (Koepke et al., 2018; Nguyen et al., 2018, and references therein) and in the Ligurian ophiolites (Tribuzio et al., 2020) for the intrusion of felsic material.

Various processes have been invoked for the formation of felsic material in oceanic environments, namely, (i) extreme MORB melt differentiation (e.g., Koepke et al., 2018; Nguyen et al., 2018; Tribuzio et al., 2020); (ii) partial melting of preexisting hydrothermally altered gabbroic rocks (e.g., France et al., 2009; Koepke et al., 2004, 2007); and (iii) liquid immiscibility of tholeiitic melts (e.g., Charlier et al., 2013). Partial melting of hydrothermally altered gabbroic rocks is expected to form a FeO- and TiO_2-depleted felsic melt (Koepke et al., 2004, 2007) as the result of the depletion of these elements within cumulate gabbros during hydrothermal alteration. The occurrence of Fe-Ti oxides and amphibole in the reaction rims suggests that the percolating felsic melt was relatively rich in Fe and Ti. This is in further agreement with the shift of the relict clinopyroxene toward lower Mg values in hybridized gabbro, also indicating high Fe concentrations in the percolating melt. In addition, the magmatic amphiboles from the felsic veins in this study show edenitic to hornblende compositions (Figure 9a), locally extending to high TiO_2 (0.54–2.00 wt%) and high Al_2O_3 contents (5.40–9.19 wt%). Similar amphiboles were documented within the diffuse felsic veins in the Atlantis Bank (Koepke et al., 2018; Nguyen et al., 2018), mostly interpreted to be products of extreme fractional crystallization. However, textural observations indicate that the amphibolite-facies deformation predated the emplacement of the felsic veins, thus suggesting that localized hydrothermal alteration of the host gabbros preceded the intrusion of felsic material (Figure 10). Based on these data, we suggest that an origin of the Si-rich melt from hydrous partial melting of hydrothermally altered gabbros is unlikely but cannot be excluded.

We note that although felsic veins at the Mado Megamullion were not observed in association with oxide gabbros, these two lithotypes have similar plagioclase compositions (Figure 7a), thus suggesting an intricate relationship of their parental melts. For instance, liquid immiscibility could have produced both an SiO_2-rich melt producing felsic veins and a ferric melt forming the oxide gabbros. The high viscosity of the SiO_2-rich melts would have prevented their lateral percolation toward the segment edge, therefore explaining the absence of felsic veins at the transform wall (see also Dick, Kvassnes, et al., 2019). However, it is noteworthy that liquid immiscibility has never been documented under hydrous conditions (e.g., Koepke et al., 2007), which is the case of the parental melts of the Mado Megamullion gabbros. On this basis, we discard liquid immiscibility as a potential candidate for the formation of the studied felsic veins. Although we retain hydrous partial melting of gabbros deformed in amphibolite facies in the presence of water as a possible process to form part of the SiO_2-rich melts percolating the Mado Megamullion, we favor extensive differentiation of a basaltic melt as the main process leading to the formation of the felsic material.

At shallower depths, the Mado Megamullion crust was widely crosscut by amphibole-rich veins formed at high-temperature conditions (842–741°C; Figure 10) and was ultimately affected by a diffuse process of amphibolitization, associated with the static recrystallization of tremolite, hornblende, and albite at the expense of the former magmatic minerals (686–622°C; Figure 10). These late metamorphic events further confirm an intense hydrothermal activity during the progressive exhumation of the OCC on the seafloor (Figure 13c).

8. Summary and Concluding Remarks

A significant fraction of the ocean floor is created in back-arc environments, and thus, constraining the evolution of the oceanic lithosphere and the formation of the gabbroic crust in these settings is an important contribution to our understanding of global oceanic spreading. We here introduce the Mado Megamullion, an OCC recently discovered in the Shikoku Basin (Philippine Sea). Similar to OCCs at mid-ocean ridges, the Mado Megamullion is characterized by spreading-parallel surface corrugations and exposure of lower gabbroic crust and upper mantle lithologies. The gabbros show textural evidence for a multiphase event of crystal-plastic deformation, ranging from granulite-facies (929–871°C) to amphibolite-facies (847–807°C) conditions. These deformation events developed shear zones that most likely initiated at hypersolidus conditions, suggesting that high-temperature deformation developed in the presence of small melt fractions. The gabbroic crust is widely crosscut by felsic veins, partly assimilating the preexisting olivine gabbros during emplacement. They likely formed at shallower levels after extreme differentiation of the melts percolating throughout the progressively exhumed gabbroic section. This magmatic and metamorphic evolution recalls that of the lower oceanic crust from OCCs worldwide, thus demonstrating that the gabbros of the Mado Megamullion represent deep-seated intrusions progressively exhumed by detachment faulting.

The gabbroic rocks show compositional features recalling those of gabbroic cumulates from MORB-type melts. However, chemical differences with gabbros from the Pacific, Atlantic, and Indian oceans suggest that the lower crust at the Mado Megamullion followed different crystal lines of descent in respect to that formed at mid-ocean ridges. We infer that the latter is controlled by phase saturation, triggered by the presence of higher water contents in the primary melts. This led to early saturation of clinopyroxene, Fe-Ti oxides, and amphibole, which in turn lowered the melt $CaO/(CaO + Na_2O)$, TiO_2 and Al_2O_3 contents compared to melts evolving at mid-ocean ridges. This difference is well depicted by the gabbros in the plagioclase anorthite versus clinopyroxene Mg-value space. The same compositional features were previously documented in gabbros from the Godzilla Megamullion and the Mariana Trough, the only known examples of lower crust formed in back-arc settings. By analogy, we infer that the water-rich character of the primary magmas produced in back-arc basins causes a distinctive crystal line of descent that could be used as a model for identifying back-arc-derived lower crustal oceanic rocks in the geological record, for example, in ophiolites.

Data Availability Statement

The geochemical data used in this study are included as tables in the supporting information. The data published are available as part of the Petrological Database (www.earthchem.org/petdb).

Acknowledgments

We thank M.-A. Kaczmarek and an anonymous reviewer for constructive reviews that improved the quality of this manuscript and M. Edmonds for her work as editor. We thank the captains and ship crews of the R/V Hakuho-Maru and R/V Yokosuka and the science teams during cruises KH07-02, KH-18-2, YK18-07, and YK19-04S. We also thank the operational team of DSV Shinkai6500 during cruises YK18-07 and YK19-04S. Special thanks to Atmosphere and Ocean Research Institute, University of Tokyo, and Japan Agency for Earth-Marine Science and Technology for their support of the aforementioned cruises. We also thank Andrea Risplendente for assistance with EPMA analyses at Università degli Studi di Milano, Italy. This research has been supported by the Italian Ministry of Education, University and Research (MIUR) through Grant PRIN 2017 Prot.2017KX5ZX8 and by the Japan Society for the Promotion of Science Grants-in-Aid for Scientific Research (Kiban-S 16H06347).

References

Agar, S. M., & Lloyd, G. E. (1997). Deformation of Fe-Ti oxides in gabbroic shear zones from the MARK area. In J. A. Karson, M. Cannat, D. J. Miller, D. Elthon (Eds.), *Proceedings of the Ocean Drilling Program, scientific results* (pp. 123–135). Ocean Drilling Program: College Station, TX.

Anderson, J. L., & Smith, D. R. (1995). The effects of temperature and f_{O2} on the Al-in-hornblende barometer. *American Mineralogist*, *80*(5–6), 549–559. https://doi.org/10.2138/am-1995-5-614

Basch, V., Rampone, E., Borghini, G., Ferrando, C., & Zanetti, A. (2019). Origin of pyroxenites in the oceanic mantle and their implications on the reactive percolation of depleted melts. *Contributions to Mineralogy and Petrology*, *174*(12), 97. https://doi.org/10.1007/s00410-019-1640-0

Basch, V., Rampone, E., Crispini, L., Ferrando, C., Ildefonse, B., & Godard, M. (2019). Multi-stage reactive formation of troctolites in slow-spreading oceanic lithosphere (Erro-Tobbio, Italy): A combined field and petrochemical study. *Journal of Petrology*, *60*(5), 873–906. https://doi.org/10.1093/petrology/egz019

Berndt, J., Koepke, J., & Holtz, F. (2005). An experimental investigation of the influence of water and oxygen fugacity on differentiation of MORB at 200 MPa. *Journal of Petrology*, *46*(1), 135–167. https://doi.org/10.1093/petrology/egh066

Bird, P. (2003). An updated digital model of plate boundaries. *Geochemistry, Geophysics, Geosystems*, *4*(3), 1027. https://doi.org/10.1029/2001GC000252

Blackman, D. K., Cann, J. R., Janssen, B., & Smith, D. K. (1998). Origin of extensional core complexes: Evidence from the Mid-Atlantic Ridge at Atlantis fracture zone. *Journal of Geophysical Research*, *103*(B9), 21,315–21,333. https://doi.org/10.1029/98JB01756

Blackman, D. K., Ildefonse, B., John, B. E., Ohara, Y., MacLeod, C. J., & Expedition 304/305 Scientists (2006). Proceedings of the Integrated Ocean Drilling Program 304–305. https://doi.org/10.2204/iodp.-proc.304305.302006

Blackman, D. K., Ildefonse, B., John, B. E., Ohara, Y., Miller, D. J., Abe, N., et al. (2011). Drilling constraints on lithospheric accretion and evolution at Atlantis massif, Mid-Atlantic Ridge 30°N. *Journal of Geophysical Research*, *116*, B07103. https://doi.org/10.1029/2010JB007931

Bloomer, S. H., Taylor, B., MacLeod, C. J., Stern, R. J., Fryer, P., Hawkins, J., & Johnson, L. (1995). Early arc volcanism and ophiolite problem: A perspective from drilling in the Western Pacific. In B. Taylor & J. Natland (Eds.), *Active margins and marginal basins of the Western Pacific*, *Geophysical Monograph* (Vol. 88, pp. 1–30). Washington, DC: American Geophysical Union. https://doi.org/10.1029/GM088p0001

Botcharnikov, R. E., Almeev, R., Koepke, J., & Holtz, F. (2008). Phase relations and liquid lines of descent in hydrous ferrobasalt—Implications for the Skaergaard intrusion and Columbia River flood basalts. *Journal of Petrology*, *49*(9), 1687–1727. https://doi.org/10.1093/petrology/egn043

Cann, J. R., Blackman, D. K., Smith, D. K., McAllister, E., Janssen, B., Mello, S., et al. (1997). Corrugated slip surfaces formed at ridge-transform intersections on the Mid-Atlantic Ridge. *Nature*, *385*(6614), 329–332. https://doi.org/10.1038/385329a0

Charlier, B., Namur, O., & Grove, T. L. (2013). Compositional and kinetic controls on liquid immiscibility in ferrobasalt-rhyolite volcanic and plutonic series. *Geochimica et Cosmochimica Acta*, *113*, 79–93. https://doi.org/10.1016/j.gca.2013.03.017

Collier, M. L., & Kelemen, P. B. (2010). The case for reactive crystallization at mid-ocean ridges. *Journal of Petrology*, *51*(9), 1913–1940. https://doi.org/10.1093/petrology/egq043

Coogan, L. A., Jenkin, G. R. T., & Wilson, R. N. (2007). Contrasting cooling rates in the lower oceanic crust at fast- and slow-spreading ridges revealed by geospeedometry. *Journal of Petrology*, *48*(11), 2211–2231. https://doi.org/10.1093/petrology/egm057

Coogan, L. A., Thompson, G., MacLeod, C. J., Dick, H. J. B., Edwards, S. J., Hosford Scheirer, A., & Barry, T. L. (2004). A combined basalt and peridotite perspective on 14 million years of melt generation at the Atlantis Bank segment of the Southwest Indian Ridge: Evidence for temporal changes in mantle dynamics? *Chemical Geology*, *207*(1–2), 13–30. https://doi.org/10.1016/j.chemgeo.2004.01.016

Coogan, L. A., Wilson, R. N., Gillis, K. M., & MacLeod, C. J. (2001). Near-solidus evolution of oceanic gabbros: Insights from amphibole geochemistry. *Geochimica et Cosmochimica Acta*, *65*(23), 4339–4357. https://doi.org/10.1016/S0016-7037(01)00714-1

Dick, H. J. B., Fisher, R. L., & Bryan, W. B. (1984). Mineralogic variability of the uppermost mantle along mid-ocean ridges. *Earth and Planetary Science Letters*, *69*(1), 88–106. https://doi.org/10.1016/0012-821X(84)90076-1

Dick, H. J. B., Kvassnes, A. J. S., Robinson, P. T., MacLeod, C. J., & Kinoshita, H. (2019). The Atlantis Bank Gabbro Massif, Southwest Indian Ridge. *Progress in Earth and Planetary Science*, *6*(1), 64. https://doi.org/10.1186/s40645-019-0307-9

Dick, H. J. B., MacLeod, C. J., Blum, P., Abe, N., Blackman, D. K., Bowles, J. A., et al. (2019). Dynamic accretion beneath a slow-spreading ridge segment: IODP Hole 1473A and the Atlantis Bank Oceanic Core Complex. *Journal of Geophysical Research*, *124*, 12,631–12,659. https://doi.org/10.1029/2018JB016858

Dick, H. J. B., & Natland, J. H. (1996). Late stage melt evolution and transport in the shallow mantle beneath the East Pacific Rise. In K. Gillis, C. Mével, J. Allan (Eds.), *Proceedings of the Ocean Drilling Program*, *Scientific Results* (Vol. 147, pp. 103–134). College Station, TX: Ocean Drilling Program.

Dick, H. J. B., Natland, J. H., Alt, J. C., Bach, W., Bideau, D., Gee, J. S., et al. (2000). A long in situ section of the lower ocean crust: Results of ODP Leg 176 drilling at the Southwest Indian Ridge. *Earth and Planetary Science Letters*, *179*(1), 31–51. https://doi.org/10.1016/S0012-821X(00)00102-3

Dick, H. J. B., Natland, J. H., & Ildefonse, B. (2006). Past and future impact of deep drilling in the oceanic crust and mantle. *Oceanography*, *19*(4), 72–80. https://doi.org/10.5670/oceanog.2006.06

Dick, H. J. B., Ozawa, K., Meyer, P. S., Niu, Y., Robinson, P. T., Constantin, M., et al. (2002). Primary silicate mineral chemistry of a 1.5-km section of very slow spreading lower ocean crust: ODP Hole 753B, Southwest Indian Ridge. *Proceedings of the Ocean Drilling Program*, *176*, 1–61. https://doi.org/10.2973/odp.proc.sr.176.001.2002

Dick, H. J. B., Tivey, M. A., & Tucholke, B. E. (2008). Plutonic foundation of a slow-spreading ridge segment: Oceanic core complex at Kane Megamullion, 23°30′N, 45°20′W. *Geochemistry, Geophysics, Geosystems*, *9*, Q05014. https://doi.org/10.1029/2007GC001645

Drouin, M., Godard, M., Ildefonse, B., Bruguier, O., & Garrido, C. (2009). Geochemical and petrographic evidence for magmatic impregnation in the oceanic lithosphere at Atlantis Massif, Mid-Atlantic Ridge (IODP Hole U1309D, 30°N). *Chemical Geology*, *264*(1–4), 71–88. https://doi.org/10.1016/j.chemgeo.2009.02.013

Escartìn, J., Mével, C., Petersen, S., Bonnemains, D., Cannat, M., Andreani, M., et al. (2017). Tectonic structure, evolution, and the nature of oceanic core complexes and their detachment fault zones (13°20′N and 13°30′N, Mid Atlantic Ridge). *Geochemistry, Geophysics, Geosystems*, *18*, 1451–1482. https://doi.org/10.1002/2016GC006775

Escartìn, J., Smith, D. K., Cann, J., Schouten, H., Langmuir, C. H., & Escrig, S. (2008). Central role of detachment faults in accretion of slow-spreading oceanic lithosphere. *Nature*, *455*(7214), 790–794. https://doi.org/10.1038/nature07333

Feig, S., Koepke, J., & Snow, J. (2006). Effect of water on tholeiitic basalt phase equilibria: An experimental study under oxidizing conditions. *Contributions to Mineralogy and Petrology*, *152*, 611–638. https://doi.org/10.1007/s00410-006-0123-2

Ferrando, C., Godard, M., Ildefonse, B., & Rampone, E. (2018). Melt transport and mantle assimilation at Atlantis Massif (IODP Site U1309): Constraints from geochemical modelling. *Lithos*, *323*, 24–43.

Ferrando, C., Lynn, K., Basch, V., Godard, M., & Ildefonse, B. (2020). Retrieving timescales of crustal evolution and mantle dynamics from geochemical profiles: The case of Atlantis Massif (IODP Site U1309D, MAR 30°N). *Lithos*, *374–375*, 105727. https://doi.org/10.1016/j.lithos.2020.105727

France, L., Ildefonse, B., & Koepke, J. (2009). Interactions between magma and hydrothermal system in Oman ophiolite and in IODP Hole 1256D: Fossilization of a dynamic melt lens at fast spreading ridges. *Geochemistry, Geophysics, Geosystems*, *10*, Q10O19. https://doi.org/10.1029/2009GC002652

Gale, A., Dalton, C. A., Langmuir, C. H., Su, Y., & Schilling, J.-G. (2013). The mean composition of ocean ridge basalts. *Geochemistry, Geophysics, Geosystems*, *14*, 489–518. https://doi.org/10.1029/2012GC004334

Ghiorso, M. S., Hirschmann, M. M., Reiners, P. W., & Kress, V. C. III (2002). The pMELTS: An revision of MELTS aimed at improving calculation of phase relations and major element partitioning involved in partial melting of the mantle at pressures up to 3 GPa. *Geochemistry, Geophysics, Geosystems*, *3*(5), 1030. https://doi.org/10.1029/2001GC000217

Gualda, G. A. R., Ghiorso, M. S., Lemons, R. V., & Carley, T. L. (2012). Rhyolite-MELTS: A modified calibration of MELTS optimized for silica-rich, fluid-bearing magmatic systems. *Journal of Petrology*, *53*(5), 875–890. https://doi.org/10.1093/petrology/egr080

Hansen, L. N., Cheadle, M. J., John, B. E., Swapp, S. M., Dick, H. J. B., Tucholke, B. E., & Tivey, M. A. (2013). Mylonitic deformation at the Kane oceanic core complex: Implications for the rheological behavior of oceanic detachment faults. *Geochemistry, Geophysics, Geosystems*, *14*, 3085–3108. https://doi.org/10.1002/ggge.20184

Harigane, Y., Michibayashi, K., & Ohara, Y. (2008). Shearing within lower crust during progressive retrogression: Structural analysis of gabbroic rocks from the Godzilla Megamullion, an oceanic core complex in the Parece Vela backarc basin. *Tectonophysics*, *457*(3–4), 183–196. https://doi.org/10.1016/j.tecto.2008.06.009

Harigane, Y., Michibayashi, K., & Ohara, Y. (2010). Amphibolitization within the lower crust in the termination area of the Godzilla Megamullion, an oceanic core complex in the Parece Vela Basin. *Island Arc*, *19*(4), 718–730. https://doi.org/10.1111/j.1440-1738.2010.00741.x

Harigane, Y., Michibayashi, K., & Ohara, Y. (2011). Deformation and hydrothermal metamorphism of gabbroic rocks within the Godzilla Megamullion, Parece Vela Basin, Philippine Sea. *Lithos*, *124*(3–4), 185–199. https://doi.org/10.1016/j.lithos.2011.02.001

Harigane, Y., Okamoto, A., Morishita, T., Snow, J. E., Tamura, A., Yamashita, H., et al. (2019). Melt-fluid infiltration along detachment shear zones in oceanic core complexes: Insights from amphiboles in gabbro mylonites from the Godzilla Megamullion, Parece Vela Basin, the Philippine Sea. *Lithos*, *344–345*, 217–231. https://doi.org/10.1016/j.lithos.2019.06.019

Holland, T., & Blundy, J. (1994). Non-ideal interactions in calcic amphiboles and their bearing on amphibole-plagioclase thermometry. *Contributions to Mineralogy and Petrology*, *116*(4), 433–447. https://doi.org/10.1007/BF00310910

Husen, A., Almeev, R. R., & Holtz, F. (2016). The effect of H_2O and pressure on multiple saturation and liquid lines of descent in basalt from the Shatsky Rise. *Journal of Petrology*, *57*(2), 309–344. https://doi.org/10.1093/petrology/egw008

Ildefonse, B., Blackman, D. K., John, B. E., Ohara, Y., Miller, D. J., MacLeod, C. J., & Integrated Ocean Drilling Program Expeditions 304/305 Science Party (2007). Oceanic core complexes and crustal accretion at slow-spreading ridges. *Geology*, *35*(7), 623–626. https://doi.org/10.1130/G23531A.1

Ildefonse, B., Christie, D. M., & Mission Moho Workshop Steering Committee (2007). Mission Moho workshop: Drilling through the oceanic crust to the mantle. *Scientific Drilling, Workshop Reports*, *4*(4, March 2007), 11–18. https://doi.org/10.2204/iodp.sd.4.02.2007

Ishizuka, O., Taylor, R. N., Umino, S., & Kanayama, K. (2020). Geochemical evolution of arc and slab following subduction initiation: A record from the Bonin Islands, Japan. *Journal of Petrology*. https://doi.org/10.1093/petrology/egaa050

Ishizuka, O., Yuasa, M., Taylor, R. N., & Sakamoto, I. (2009). Two contrasting magmatic types coexist after the cessation of back-arc spreading. *Chemical Geology*, *266*(3–4), 274–296. https://doi.org/10.1016/j.chemgeo.2009.06.014

Karson, J. A. (1990). Seafloor spreading on the Mid-Atlantic Ridge: Implications for the structure of ophiolites and oceanic lithosphere produced in slow-spreading environments. In J. Malpas, et al. (Eds.), *Ophiolites and oceanic crustal analogues: Proceedings of the symposium "Troodos 1987"* (pp. 125–130). Nicosia, Cyprus: Geological Survey Department.

Kelemen, P. B., Kikawa, E., Miller, D. J., & Expedition 209 Scientist (2004). *Proceedings of the Ocean Drilling Program, initial reports* (Vol. 209). College Station, TX: Texas A&M University, Ocean Drilling Program. https://doi.org/10.2973/odp.proc.ir.209.2004

Kempton, P. D., & Casey, J. F. (1997). Petrology and geochemistry crosscutting diabase dikes, Sites 920 and 921. In J. A. Karson, M. Cannat, D. J. Miller, D. Elthon (Eds.), *Proceedings of Ocean Drilling Project, scientific results* (Vol. 153, pp. 363–379). Ocean Drilling Program: College Station, TX. https://doi.org/10.2973/odp.proc.sr.153.030.1997

Kessel, R., Schmidt, M. W., Ulmer, P., & Pettke, T. (2005). Trace element signature of subduction-zone fluids, melts and supercritical liquids at 120–180 km depth. *Nature*, *437*(7059), 724–727. https://doi.org/10.1038/nature03971

Klein, E. M., & Langmuir, C. H. (1987). Global correlations of ocean ridge basalt chemistry with axial depth and crustal thickness. *Journal of Geophysical Research*, *92*(B8), 8089–8115. https://doi.org/10.1029/JB092iB08p08089

Kobayashi, K., Kasuga, S., & Okino, K. (1995). Shikoku basin and its margins. In B. Taylor (Ed.), *Back-Arc Basins* (pp. 381–405). New York: Plenum. https://doi.org/10.1007/978-1-4615-1843-3_10

Koepke, J., Berndt, S. T. F., & Holtz, F. (2007). The formation of SiO_2-rich melts within the deep oceanic crust by hydrous partial melting of gabbros. *Contributions to Mineralogy and Petrology*, *153*(1), 67–84. https://doi.org/10.1007/s00410-006-0135-y

Koepke, J., Botcharnikov, R. E., & Natland, J. H. (2018). Crystallization of late-stage MORB under varying water activities and redox conditions: Implications for the formation of highly evolved lavas and oxide gabbro in the ocean crust. *Lithos*, *323*, 58–77. https://doi.org/10.1016/j.lithos.2018.10.001

Koepke, J., Feig, S. T., Snow, J., & Freise, M. (2004). Petrogenesis of oceanic plagiogranites by partial melting of gabbros: An experimental study. *Contributions to Mineralogy and Petrology*, *146*(4), 414–432. https://doi.org/10.1007/s00410-003-0511-9

Koepke, J., France, L., Müller, T., Faure, F., Goetze, N., Dziony, W., & Ildefonse, B. (2011). Gabbros from IODP Site 1256, equatorial Pacific: Insight into axial magma chamber processes at fast spreading ocean ridges. *Geochemistry, Geophysics, Geosystems*, *12*, Q09014. https://doi.org/10.1029/2011GC003655

Koepke, J., Schoenborn, S., Oelze, M., Wittmann, H., Feig, S. T., Hellebrand, E., et al. (2009). Petrogenesis of crustal wehrlites in the Oman ophiolite: Experiments and natural rocks. *Geochemistry, Geophysics, Geosystems*, *10*, Q10002. https://doi.org/10.1029/2009GC002488

Leake, B. E., Woolley, A. R., Arps, C. E. S., Birch, W. D., Gilbert, M. C., Grice, J. D., et al. (1997). Nomenclature of amphiboles: Report of the subcommittee on amphiboles of the International Mineralogical Association Commission on New Minerals and Mineral Names. *The Canadian Mineralogist*, *35*, 219–246.

Lissenberg, C. J., Howard, K. A., MacLeod, C. J., & Godard, M. (2013). Pervasive reactive melt migration through fast-spreading lower oceanic crust (Hess Deep, equatorial Pacific Ocean). *Earth and Planetary Science Letters*, *361*, 436–447. https://doi.org/10.1016/j.epsl.2012.11.012

Loocke, M., Snow, J. E., & Ohara, Y. (2013). Melt stagnation in peridotites from the Godzilla Megamullion Oceanic Core Complex, Parece Vela Basin, Philippine Sea. *Lithos*, *182–183*, 1–10. https://doi.org/10.1016/j.lithos.2013.09.005

MacLeod, C. J., Dick, H. J. B., Blum, P., & the Expedition 360 Scientists (2017). Southwest Indian Ridge Lower Crust and Moho. Proceedings of the Integrated Ocean Drilling Program, p. 360. https://doi.org/10.14379/iodp.proc.14360.14103.12017

MacLeod, C. J., Lissenberg, C. J., & Bibby, L. E. (2013). "Moist MORB" axial magmatism in the Oman ophiolite: The evidence against a mid-ocean ridge origin. *Geology*, *41*(4), 459–462. https://doi.org/10.1130/G33904.1

MacLeod, C. J., Searle, R. C., Murton, B. J., Casey, J. F., Mallows, C., Unsworth, S. C., et al. (2009). Life cycle of oceanic core complexes. *Earth and Planetary Science Letters*, *287*(3–4), 333–344. https://doi.org/10.1016/j.epsl.2009.08.016

Mehl, L., & Hirth, G. (2008). Plagioclase preferred orientation in layered mylonites: Evaluation of flow laws for the lower crust. *Journal of Geophysical Research*, *113*, B05202. https://doi.org/10.1029/2007JB005075

Michibayashi, K., Harigane, Y., Ohara, Y., Muto, J., & Okamoto, A. (2014). Rheological properties of the detachment shear zone of an oceanic core complex inferred by plagioclase flow law: Godzilla Megamullion, Parece Vela back-arc basin, Philippine Sea. *Earth and Planetary Science Letters*, *408*, 16–23. https://doi.org/10.1016/j.epsl.2014.10.005

Michibayashi, K., Watanabe, T., Harigane, Y., & Ohara, Y. (2016). The effect of a hydrous phase on P-wave velocity anisotropy within a detachment shear zone in the slow-spreading oceanic crust: A case study from the Godzilla Megamullion, Philippine Sea. *Island Arc*, *25*(3), 209–219. https://doi.org/10.1111/iar.12132

Miller, D. J., Abratis, M., Christie, D., Drouin, M., Godard, M., Ildefonse, B., et al. (2009). In D. K. Blackman et al. (Eds.), *Data report: Microprobe analyses of primary mineral phases from site U1309, Atlantis Massif, IODP Expedition 304/305* (Vol. 304/305, p. 4). Paper presented at Proceedings of the Integrated Ocean Drilling Program, College Station, TX. https://doi.org/10.2204/iodp.proc.304305.202.2009

Miranda, E. A., & John, B. E. (2010). Strain localization along the Atlantis Bank oceanic detachment fault system, southwest Indian ridge. *Geochemistry, Geophysics, Geosystems*, *11*, Q04002. https://doi.org/10.1029/2009GC002646

Natland, J. H., & Dick, H. J. B. (2002). Stratigraphy and composition of gabbros drilled at ODP Hole 735B, southwest Indian ridge: A synthesis of geochemical data. In J. H. Natland, H. J. B. Dick, D. J. Miller, R. P. von Herzen (Eds.), *Proceedings ODP, Scientific Results* (pp. 1–69). College Station, TX: Ocean Drilling Program.

Nguyen, D. K., Morishita, T., Soda, Y., Tamura, A., Ghosh, B., Harigane, Y., et al. (2018). Occurrence of felsic rocks in oceanic gabbros from IODP Hole U1473A: Implications for evolved melt migration in the lower oceanic crust. *Minerals*, *8*(12), 583. https://doi.org/10.3390/min8120583

Ohara, Y. (2016). The Godzilla Megamullion, the largest oceanic core complex on the earth: A historical review. *Island Arc*, *25*(3), 193–208. https://doi.org/10.1111/iar.12116

Ohara, Y., Fujioka, K., Ishii, T., & Yurimoto, H. (2003). Peridotites and gabbros from the Parece Vela back-arc basin: Unique tectonic window in an extinct back-arc spreading ridge. *Geochemistry, Geophysics, Geosystems*, *4*(7), 8611. https://doi.org/10.1029/2002GC000469

Ohara, Y., Kato, Y., Yoshida, T., & Nishimura, A. (2015). Geoscientific characteristics of the seafloor of the southern ocean of Japan revealed by Japan's Continental Shelf Survey. *Journal of Geography*, *124*(5), 687–709. https://doi.org/10.5026/jgeography.124.687 (in Japanese with English abstract)

Ohara, Y., Okino, K., Akizawa, N., Fujii, M., Harigane, Y., Hirano, N., et al. (2019) Introducing an oceanic core complex in the Shikoku Basin: Mado Megamullion. Japan Geoscience Union Meeting, SP30–SP07.

Ohara, Y., Okino, K., Akizawa, N., Fujii, M., Harigane, Y., Hirano, N., et al. (2018) A new tectonic window into the backarc basin lower oceanic crust and upper mantle: Mado Megamullion in the Shikoku Basin. AGU Fall Meeting, T32C-05B, Washington, DC, USA.
Ohara, Y., Okino, K., & Snow, J. (2011). Tectonics of unusual crustal accretion in the Parece Vela Basin. In Y. Ogawa et al. (Eds.), *Accretionary prisms and convergent margin*, *Tectonics in the Northwest Pacific Basin, Modern Approaches in Solid Earth Sciences* (Vol. 8, pp. 149–168). Dordrecht: Springer. https://doi.org/10.1007/978-90-481-8885-7_7
Ohara, Y., & Snow, J. E. (2009). Godzilla Mullion: Current understanding on the nature of the world's largest oceanic core complex. EOS Transactions, AGU 90(52), fall meeting supplement, T33D-06, San Francisco, USA.
Ohara, Y., Stern, R. J., Ishii, T., Yurimoto, H., & Yamazaki, T. (2002). Peridotites from the Mariana Trough: First look at the mantle beneath an active back-arc basin. *Contributions to Mineralogy and Petrology*, *143*(1), 1–18. https://doi.org/10.1007/s00410-001-0329-2
Ohara, Y., Yoshida, T., Kato, Y., & Kasuga, S. (2001). Giant Megamullion in the Parece Vela Backarc basin. *Marine Geophysical Research*, *22*(1), 47–61. https://doi.org/10.1023/A:1004818225642
Okino, K., Kasuga, S., & Ohara, Y. (1998). A new scenario of the Parece Vela basin genesis. *Marine Geophysical Research*, *20*(1), 21–40. https://doi.org/10.1023/A:1004377422118
Okino, K., Ohara, Y., Fujii, M., & Hanyu, T. (2019). Evolution of oceanic core complexes in the Shikoku Basin: When backarc basins cease to open. Japan Geoscience Union Meeting, SCG56-P06.
Okino, K., Ohara, Y., Kasuga, S., & Kato, Y. (1999). The Philippine Sea: New survey results reveal the structure and the history of the marginal basin. *Geophysical Research Letters*, *26*(15), 2287–2290. https://doi.org/10.1029/1999GL900537
Okino, K., Shimakawa, Y., & Nagaoka, S. (1994). Evolution of the Shikoku basin. *Journal of Geomagnetism and Geoelectricity*, *46*(6), 463–479. https://doi.org/10.5636/jgg.46.463
Olive, J.-A., Behn, M. D., & Tucholke, B. E. (2010). The structure of oceanic core complexes controlled by the depth distribution of magma emplacement. *Nature Geoscience*, *3*(7), 491–495. https://doi.org/10.1038/ngeo888
Otten, M. T. (1984). The origin of brown hornblende in the Artfjället gabbro and dolerites. *Contributions to Mineralogy and Petrology*, *86*(2), 189–199. https://doi.org/10.1007/BF00381846
Parnell-Turner, R., Escartín, J., Olive, J. A., Smith, D. K., & Petersen, S. (2018). Genesis of corrugated 390 fault surfaces by strain localization recorded at oceanic detachments. *Earth and Planetary Science Letters*, *498*, 116–128. https://doi.org/10.1016/j.epsl.2018.06.034
Pearce, J. A. (2003). Supra-subduction zone ophiolites: The search for modern analogues. *Geological Society of America Special Papers*, *373*, 269–293. https://doi.org/10.1130/0-8137-2373-6.269
Putirka, K. (2016). Amphibole thermometers and barometers for igneous systems and some implications for eruption mechanisms of felsic magmas at arc volcanoes. *American Mineralogist*, *101*(4), 841–858. https://doi.org/10.2138/am-2016-5506
Ridolfi, F., & Renzulli, A. (2011). Calcic amphiboles in calc-alkaline and alkaline magmas: Thermobarometric and chemometric empirical equations valid up to 1,130°C and 2.2 GPa. *Contributions to Mineralogy and Petrology*, *163*(5), 877–895. https://doi.org/10.1007/s00410-011-0704-6
Sanfilippo, A., Dick, H. J. B., Marschall, H. R., Lissenberg, C. J., & Urann, B. (2018). Emplacement and high-temperature evolution of gabbros of the 16.5°N oceanic core complexes (Mid-Atlantic Ridge): Insights into the compositional variability of the lower oceanic crust. *Geochemistry, Geophysics, Geosystems*, *20*, 46–66. https://doi.org/10.1029/2018GC007512
Sanfilippo, A., Dick, H. J. B., & Ohara, Y. (2013). Melt-rock reaction in the mantle: Mantle troctolites from the Parece Vela Ancient Back-Arc Spreading Center. *Journal of Petrology*, *54*(5), 861–885. https://doi.org/10.1093/petrology/egs089
Sanfilippo, A., Dick, H. J. B., Ohara, Y., & Tiepolo, M. (2016). New insights on the origin of troctolites from the breakaway area of the Godzilla Megamullion (Parece Vela back-arc basin): The role of melt mantle interaction on the composition of the lower crust. *Island Arc*, *25*(3), 220–234. https://doi.org/10.1111/iar.12137
Sanfilippo, A., & Tribuzio, R. (2011). Melt transport and deformation history in a nonvolcanic ophiolitic section, northern Apennines, Italy: Implications for crustal accretion at slow spreading settings. *Geochemistry, Geophysics, Geosystems*, *12*, Q0AG04. https://doi.org/10.1029/2010GC003429
Sauter, D., Cannat, M., Rouméjon, S., Andreani, M., Birot, D., Bronner, A., et al. (2013). Continuous exhumation of mantle-derived rocks at the Southwest Indian Ridge for 11 million years. *Nature Geoscience*, *6*(4), 314–320. https://doi.org/10.1038/ngeo1771
Schroeder, T., & John, B. (2004). Strain localization on an oceanic detachment fault system, Atlantis Massif, 30°N, Mid-Atlantic Ridge. *Geochemistry, Geophysics, Geosystems*, *5*, Q11007. https://doi.org/10.1029/2004GC000728
Sdrolias, M., & Müller, R. D. (2006). Controls on back-arc basin formation. *Geochemistry, Geophysics, Geosystems*, *7*, Q04016. https://doi.org/10.1029/2005GC001090
Sdrolias, M., Roest, W. R., & Müller, R. D. (2004). An expression of Philippine Sea plate rotation: The Parece Vela and Shikoku basins. *Tectonophysics*, *394*(1–2), 69–86. https://doi.org/10.1016/j.tecto.2004.07.061
Shervais, J. W., & Jean, M. M. (2012). Inside the subduction factory: Modeling fluid mobile element enrichment in the mantle wedge above a subduction zone. *Geochimica et Cosmochimica Acta*, *95*, 270–285. https://doi.org/10.1016/j.gca.2012.07.006
Sisson, T. W., & Grove, T. L. (1993). Experimental investigations of the role of H_2O in calc-alkaline differentiation and subduction zone magmatism. *Contributions to Mineralogy and Petrology*, *113*(2), 143–166. https://doi.org/10.1007/BF00283225
Smith, D. K., Escartin, J., Schouten, H., & Cann, J. R. (2008). Fault rotation and core complex formation: Significant processes in seafloor formation at slow-spreading mid-ocean ridges (Mid-Atlantic Ridge, 13°–15°N). *Geochemistry, Geophysics, Geosystems*, *9*, Q03003. https://doi.org/10.1029/2007GC001699
Smith, D. K., Schouten, H., Dick, H. J. B., Cann, J. R., Salters, V., Marschall, H. R., et al. (2014). Development and evolution of detachment faulting along 50 km of the Mid-Atlantic Ridge near 16.5°N. *Geochemistry, Geophysics, Geosystems*, *15*, 4692–4711. https://doi.org/10.1002/2014GC005563
Spencer, J. E., & Ohara, Y. (2014). Curved grooves at the Godzilla Megamullion in the Philippine Sea and their tectonic significance. *Tectonics*, *33*, 1028–1038. https://doi.org/10.1002/2013TC003515
Stern, R. J., Bloomer, S. H., Martinez, F., Yamazaki, T., & Harrison, T. M. (1996). The composition of back-arc basin lower crust and upper mantle in the Mariana Trough: A first report. *Island Arc*, *5*(3), 354–372. https://doi.org/10.1111/j.1440-1738.1996.tb00036.x
Stern, R. J., Yamazaki, T., Danishwar, S., & Sun, C.-H. (1997). Back-arc basin lower crust and upper mantle in the northern Mariana Trough studied with "Shinkai 6500". *JAMSTEC Japanese Deep Sea Research*, *13*, 47–61.
Suhr, G., Hellebrand, E., Johnson, K., & Brunelli, D. (2008). Stacked gabbro units and intervening mantle: A detailed look at a section of IODP Leg 305, Hole U1309D. *Geochemistry, Geophysics, Geosystems*, *9*, Q10007. https://doi.org/10.1029/2008GC002012
Taira, A., Ohara, Y., Wallis, S. R., Ishiwatari, A., & Iryu, Y. (2016). Geological evolution of Japan: an overview. In T. Moreno, et al. (Eds.), *The Geology of Japan* (pp. 1–24). London: Geological Society of London. https://doi.org/10.1144/GOJ.1

10.1029/2020GC009199

Tani, K., Dunkley, D., & Ohara, Y. (2011). Termination of backarc spreading: Zircon dating of a giant oceanic core complex. *Geology*, *39*(1), 47–50. https://doi.org/10.1130/G31322.1

Taylor, B., & Martinez, F. (2003). Back-arc basin basalt systematics. *Earth and Planetary Science Letters*, *210*(3–4), 481–497. https://doi.org/10.1016/S0012-821X(03)00167-5

Toplis, M. J., & Carroll, M. R. (1995). An experimental study of the influence of oxygen fugacity on Fe-Ti oxide stability, phase relations, and mineral-melt equilibria in ferro-basaltic systems. *Journal of Petrology*, *36*(5), 1137–1170. https://doi.org/10.1093/petrology/36.5.1137

Tribuzio, R., Manatschal, G., Renna, M. R., Ottolini, L., & Zanetti, A. (2020). Tectono-magmatic interplay and related metasomatism in gabbros of the Chenaillet Ophiolite (Western Alps). *Journal of Petrology*, in press, *60*(12), 2483–2508. https://doi.org/10.1093/petrology/egaa015

Tucholke, B. E., Behn, M. D., Buck, W. R., & Lin, J. (2008). Role of melt supply in oceanic detachment faulting and formation of megamullions. *Geology*, *36*(6), 455–458. https://doi.org/10.1130/G24639A.1

Tucholke, B. E., & Lin, J. (1994). A geological model for the structure of ridge segments in slow-spreading ocean crust. *Journal of Geophysical Research*, *99*(B6), 11,937–11,958. https://doi.org/10.1029/94JB00338

Tucholke, B. E., Lin, J., & Kleinrock, M. C. (1998). Megamullions and mullion structure defining oceanic metamorphic core complexes on the Mid-Atlantic Ridge. *Journal of Geophysical Research*, *103*(B5), 9857–9866. https://doi.org/10.1029/98JB00167

Workman, R. K., & Hart, S. R. (2005). Major and trace element composition of the depleted MORB mantle (DMM). *Earth and Planetary Science Letters*, *231*(1–2), 53–72. https://doi.org/10.1016/j.epsl.2004.12.005

Zhang, W., Zeng, Z., Cui, L., & Yin, X. (2018). Geochemical constrains on MORB composition and magma sources at East Pacific Rise between 1°S and 2°S. *Journal of Ocean University of China*, *17*(2), 297–304. https://doi.org/10.1007/s11802-018-3223-5